ACS Chemical Neuroscience

Article

Discovery of Selective, Substrate-Competitive, and Passive Membrane Permeable Glycogen Synthase Kinase-3# Inhibitors: Synthesis, Biological Evaluation, and Molecular Modeling of New C-Glycosylflavones

Zhibin Liang, and Qing X. Li

ACS Chem. Neurosci., **Just Accepted Manuscript** • DOI: 10.1021/acschemneuro.8b00010 • Publication Date (Web): 30 Jan 2018

ACS Publications

ACS Chemical Neuroscience is published by the American Chemical Society. 1155 Sixteenth Street N.W., Washington, DC 20036

Discovery of Selective, Substrate-Competitive, and Passive Membrane Permeable Glycogen Synthase Kinase-3β Inhibitors: Synthesis, Biological Evaluation, and Molecular Modeling of New *C*-Glycosylflavones

Zhibin Liang and Qing X. Li*

Department of Molecular Biosciences and Bioengineering, University of Hawaii at Manoa, Honolulu, Hawaii 96822, United States

ABSTRACT: Glycogen synthase kinase-3β (GSK-3β) is a key enzyme responsible for tau hyperphosphorylation and is a viable therapeutic target of Alzheimer's disease (AD). We developed a new class of GSK-3β inhibitors based on the 6-*C*-glycosylflavone isoorientin (**1**). The new inhibitors are passive membrane permeable and constitutively attenuate GSK-3β mediated tau hyperphosphorylation and amyloid neurotoxicity in an AD cellular model. Enzymatic assays and kinetic studies demonstrated that compound **30** is a GSK-3β substrate-competitive inhibitor with distinct kinase selectivity, isoform-selectivity and over 310-fold increased potency as compared to **1**. Structure-activity relationship analyses and *in silico* modeling suggest the mechanism of actions by which the hydrophobic, π-cation and orthogonal multipolar interactions of **30** with the substrate site are critical for the GSK-3β inhibition and selectivity. The results provide new insights into GSK-3β drug discovery. The new inhibitors are valuable chemical probes and drug leads with therapeutic potential to tackle AD and other GSK-3β relevant diseases.

Keywords: *C*-Glycosylflavone, computer-aided drug design, glycogen synthase kinase-3, substrate-competitive inhibitor, kinase selectivity, tauopathy, Alzheimer's disease

Introduction

Alzheimer's disease (AD) is an irreversible and progressive neurological disorder that causes memory loss, cognitive decline, and eventually death due to severe brain degeneration.[1] This devastating and fatal disease, unfortunately, cannot be prevented, cured or even slowed. Although the exact cause of AD remains unclear, increasing evidence suggests that β-amyloid (Aβ) is plausibly the pathogenic initiator of AD and tau aggregation and distribution in the brain cortices correlate closely with neuronal loss and cognitive decline in AD progression.[1-2] The tau

protein stabilizes the structural integrity of microtubules in neurons to maintain healthy axonal transport. In AD, aberrant phosphorylation of tau proteins disrupts their association, leading to destabilization of microtubules and mislocalization of the abnormal tau to the soma and dendrites.[3] The subsequent aggregation of hyperphosphorylated tau results in formation and disposition of toxic neurofibrillary tangles (NFTs), triggering synaptic dysfunction, neuronal cell death and cognitive impairment. This aberrant signaling cascade gives rise to the tauopathy in AD.[4] The continued failures of anti-Aβ approaches in AD clinical studies[5-6] drive researchers embrace an alternative approach to investigate anti-tau strategies for AD treatment.[4, 7]

Glycogen synthase kinase-3β (GSK-3β) is a key protein kinase in the cascade leading to aberrant tau hyperphosphorylation. Elevated GSK-3β activity has been implicated in AD and other tauopathies.[8] Overactive GSK-3β hyperphosphorylates over 70% of the potential phosphorylation sites on tau proteins in AD brains, which impairs the healthy interactions of tau proteins with microtubules.[9] The development of selective GSK-3β inhibitors modulating aberrant tau phosphorylation is therefore a promising strategy for AD chemotherapy.[10-11] To date, the US-FDA has approved four AD drugs, but they only ameliorate temporary symptoms, and none targets GSK-3β.[10]

Traditional GSK-3β inhibitors target the highly conserved ATP site. However, the limited selectivity of those inhibitors raises safety concerns owing to off-target effects and, therefore, remains a major challenge in GSK-3β based drug development.[11] Despite substantial efforts in developing GSK-3β inhibitors in the past decades, to date only lithium carbonate and tideglusib (a TDZD compound) have been studied in clinical trials for AD.[10] Lithium carbonate shows a weak inhibition (IC_{50}, 2 mM),[11] while tideglusib (IC_{50}, 100 nM) is an irreversible and time-dependent inhibitor of GSK-3β.[12-13] In recent years, strategies have been employed to search for

selective and reversible GSK-3β inhibitors, particularly those that are not ATP-site directed. It is known that the substrate domain of GSK-3β is less conserved with a unique folding different from other kinases.[11, 14] Inhibitors targeting this site are thought to be more specific and selective than the ATP-competitive inhibitors.[11, 14] Yet few substrate-competitive inhibitors of GSK-3β have been reported.[15-18] New, potent, selective and reversible inhibitors targeting the substrate site on GSK-3β are potential disease-modifying therapies for AD.

We have undertaken a different approach to discover potential substrate-competitive inhibitors of GSK-3β from natural sources. Natural products are valuable starting points for drug discovery as they have been naturally selected and optimized under evolutionary pressure and obtained privileged structures for protein binding.[19] *C*-Glycosylflavones and their aglycones (Figure 1) omnipresent in plants are important phytochemicals noted for anti-oxidation, anti-inflammation, anti-cancer, anti-cardiovascular diseases, and cognitive enhancement.[20-22] We recently screened corn silks for GSK-3β inhibitors and isolated a 6-*C*-glycosylflavone, isoorientin (**1**).[23] Compound **1** alleviates tau hyperphosphorylation and amyloid neurotoxicity through selective and reversible GSK-3β inhibition,[23] by which the mechanism of action is substrate competition rather than the common ATP competition.[23] In addition, a recent study showed that **1** and related natural flavones attenuate Aβ burden and neuroinflammation in an APPswe/PSEN1dE9 mouse model of AD.[24] **1** from maize crop[23] is conceivably safe as supported by *in vivo* subchronic toxicity studies of corn silk-derived flavones in mice and rats.[25] **1** is a promising medicinal natural product with a novel mode of action for reducing AD burdens.[23-25] However, the lack of druggable potency (IC_{50}, 185 μM), commonly suffered by bioactive natural products, makes it challenging in pharmaceutical applications. Potency improvement, through structure-activity relationship (SAR)-based optimization, pharmacological and pharmacokinetic evaluations, as well as testing

administration routes *in vivo* are therefore necessary to develop analogues of **1** with therapeutic potential.

In our recent paper, preliminary examination of the predicted 3D structure of the GSK-3β-**1** complex revealed that the substrate pocket of GSK-3β favors specific interactions with both the *C*-glycone and flavone moieties in **1**.[23] In particular, a cleft comprised of Phe67, Val87, Leu88 and Phe93 on GSK-3β is critical for substrate recognition.[26] This concave cleft could accommodate a hydrophobic moiety favoring ligand binding, which is in the vicinity of the primary hydroxyl group on *C*-glycone of **1**. This raises our hypothesis that introduction of a hydrophobic functional group at this primary alcohol enhances affinity and selectivity of **1** to GSK-3β. In addition, methylation of the phenolic hydroxyls can improve bioavailability, metabolic stability and potency of flavones.[27]

In the present study, a new series of **1** analogues containing a 6-*C*-glycosylflavone scaffold were semi-synthesized to target the substrate site on GSK-3β. Potency, selectivity, passive membrane permeability, anti-tau hyperphosphorylation, and anti-Aβ neurotoxicity of the new inhibitors were evaluated with molecular and cellular studies, SAR analysis and molecular modeling.

Results

Chemistry

Design and Synthesis. A series of new analogues of **1** were designed and synthesized (Table 1). The semi-synthesis of 6-*C*-glycosylflavones from **1** was carried out according to the route outlined in Scheme 1. The four phenolic hydroxyls on the flavone core of **1** were first selectively

methylated by $TMSCHN_2$ in a methanolic toluene solution according to a previously described method.[28] The resulting tetra-methylated product (**5**) then underwent an oxoammonium salt-mediated oxidation. We optimized an oxidation protocol[29] using a $[TEMPO]^+[BF_4]^-$ salt in a pyridine base solution at room temperature, which chemoselectively transformed the primary alcohol to a carboxylic acid without affecting the secondary hydroxyls on the *C*-glycone. This method successfully afforded the desired product (**6**) in over 95% yield which was confirmed by ESI-TOF-MS and NMR analyses. The carboxylic acid derivative **6** was then subjected to methyl esterification to afford **7**. It is known that an ester bond is susceptible to metabolic hydrolysis. Our chemical design was focused on amide analogues with better physiochemical stability. A small library of hydrophobic amides (**8**-**31**) was generated by coupling **6** with a series of organic amines via HCTU catalysis. Aliphatic, alicyclic, aromatic and fluorinated amines were selected for the solution-phase amidation (Table 1). The resulting hydrophobic amides were evaluated on their SAR, cytotoxicity, anti-AD activity, and passive membrane permeability. All final products were characterized by NMR and HRMS, and were over 95% purity determined by HPLC-UV at 210, 254, and 340 nm.

Table 1. Chemical Structures of Natural and Semi-Synthetic *C*-Glycosylflavones.

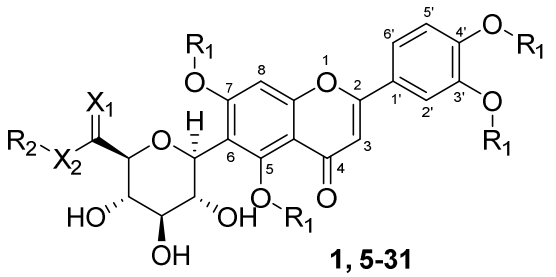

1, 5-31

cmpd no.	Functional group			
	R_1	**X_1**	**X_2**	**R_2**
1	H	H_2	O	H
5	CH_3	H_2	O	H
6	CH_3	O	O	H
7	CH_3	O	O	CH_3
8	CH_3	O	NH	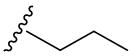
9	CH_3	O	NH	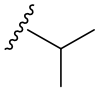
10	CH_3	O	NH	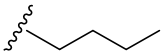
11	CH_3	O	NH	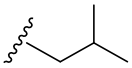
12	CH_3	O	NH	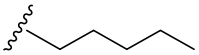
13	CH_3	O	NH	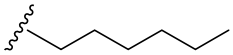
14	CH_3	O	NH	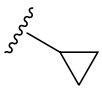
15	CH_3	O	NH	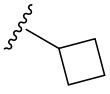
16	CH_3	O	NH	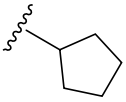

17	CH_3	O	NH	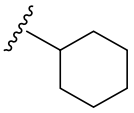
18	CH_3	O	NH	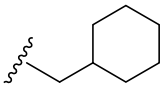
19	CH_3	O	NH	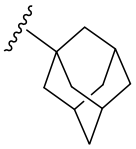
20	CH_3	O	NH	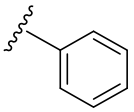
21	CH_3	O	NH	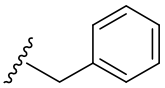
22	CH_3	O	NH	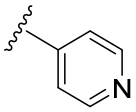
23	CH_3	O	NH	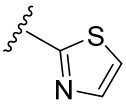
24	CH_3	O	NH	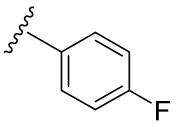
25	CH_3	O	NH	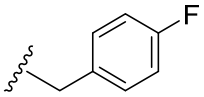
26	CH_3	O	NH	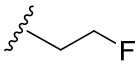
27	CH_3	O	NH	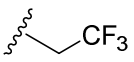
28	CH_3	O	NH	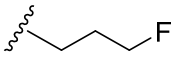
29	CH_3	O	NH	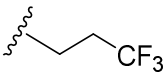
30	CH_3	O	NH	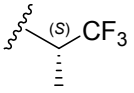
31	CH_3	O	NH	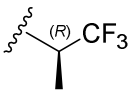

Biological Activities and Relevance

Structure-Activity Relationship and Ligand-Lipophilic Efficiency of *C*-Glycosylflavones to GSK-3β. The semi-synthetic 6-*C*-glycosylflavones (**5-31**) were assayed on GSK-3β inhibition in comparison to four natural flavones with structural similarities (two 6-*C*-glycosylflavones isoorientin **1** and isovitexin **2**, one 8-*C*-glycosylflavone orientin **3**, and a flavone aglycone luteolin **4**). Among the four flavones (**1-4**, Figure 1), **4** showed the highest potency against GSK-3β (IC_{50}, 3.1 μM in Table 2), but it is nonspecific and promiscuous as noted in the literature and our previous studies.[23, 30] **1** and **2** with *C*-glycosides at 6-position showed a moderate potency against GSK-3β with an IC_{50} value of 185 and 194 μM, respectively (Figure 1 and Table 2). In contrast, **3** with an 8-*C*-glycoside was inactive (IC_{50}, > 5 mM). The results demonstrated that the presence and position of *C*-glycone on the flavone core are critical for GSK-3β inhibition, which agrees with our previous observation.[23]

The tetra-methylated alcohol (**5**) and tetra-methylated carboxylic acid (**6**) slightly decreased the potency (IC_{50}, 237 and 239 μM, respectively) in comparison with **1**, indicating a trivial contribution of the phenolic hydroxyl groups to GSK-3β inhibition. However, a methyl ester (**7**) (IC_{50}, 135 μM) increased the potency by 1.37-fold as compared to **1** (IC_{50}, 185 μM), suggesting hydrophobic groups at the primary hydroxyl position are preferred for GSK-3β inhibition. Remarkably, transforming the primary alcohol to corresponding hydrophobic amides (**8-31**) (Table 2) significantly increased the potency against GSK-3β as most analogues displayed IC_{50} values less than 50 μM and ten of them (**9**, **13**, **16**, **17, 20, 21, 27, 29, 30** and **31**) were less than 20 μM. As shown in Figure 2A, the aliphatic (e.g., **9** and **13**) and alicyclic amides (e.g., **16** and **17**) exhibited a higher affinity to GSK-3β than the aromatic amides (e.g., **20-23**). Small (**14** and **15**) or large (**18** and **19**) alicyclic rings showed a less affinity than the cyclopentyl (**16**) or

cyclohexyl (**17**) analogues, plausibly due to the size of the hydrophobic concave cleft in the substrate site on GSK-3β. A branched isopropyl group (**9**, **30**, and **31**) showed a higher affinity than a linear propyl group (**8**, **28**, and **29**). Mono-fluorination of phenyl (**24**), benzyl (**25**), ethyl (**26**) or propyl (**28**) groups did not improve affinity as compared to non-fluorinated counterparts (e.g., **8**, **20**, and **21**). It is interesting that a trifluoromethyl (CF_3) group has a significant effect on potency. Compounds **27**, **29**, **30** and **31** containing a CF_3 moiety consistently improved binding affinity to GSK-3β in comparison with no fluorine or mono-fluorinated counterparts (e.g., **8**, **9**, **26** and **28**) (Figure 2A). In particular, **30** (IC_{50}, 0.59 μM) with a (*S*)-CF_3 group increased the potency against GSK-3β by 310-fold in comparison with **1**, and is about 4-fold more potent than its epimer **31** with a (*R*)-CF_3 group (IC_{50}, 2.3 μM). All new analogues were not pan-assay interference compounds to GSK-3β as determined with a detergent-based assay.[23, 30-31]

Ligand-lipophilic efficiency (LiPE) is a parameter commonly used in drug design to assess the quality of compound candidates. Lipophilicity is the most important druglike physiochemical property that highly correlates to absorption, distribution, metabolism, excretion and toxicity (ADMET) profiles and ultimately to the pharmacological response for oral drugs.[32] High potency (large pIC_{50}) is a desirable feature in drug candidates, as it reduces the risk of off-target and nonspecific pharmacology. Correlation between lipophilicity (CLog*P*) and potency (pIC_{50}) provides a valuable parameter to estimate druglikeness.[33] Many of the semi-synthetic analogues clustered in an upper-right range of the LiPEs between 2 and 4, indicating that both lipophilicity (CLog*P*) and GSK-3β inhibitory potency (pIC50) have been increased relative to **1** (Figure 2B). Particularly, **30** has the highest LiPE value (> 4) among the analogues, suggesting a unique contribution of the CF_3 moiety of **30** to improving potency and lipophilicity.

Table 2. Comparison of Natural and Semi-Synthetic *C*-Glycosylflavones on GSK-3β Inhibition and CLog*P*

cmpd no.	GSK-3β inhibition IC_{50} (μM) [a]	CLog*P* [b]	cmpd no.	GSK-3β inhibition IC_{50} (μM) [a]	CLog*P* [b]
1	184.9 ± 1.4	0.21	**17**	9.0 ± 1.3	2.55
2	194.1 ± 1.0	0.80	**18**	26.0 ± 1.2	3.16
3	5153 ± 31	0.21	**19**	33.5 ± 0.8	3.17
4	3.1 ± 1.3	2.31	**20**	19.7 ± 1.1	2.21
5	239.2 ± 1.2	1.28	**21**	15.8 ± 1.2	2.34
6	237.3 ± 1.4	0.80	**22**	35.6 ± 1.3	1.54
7	135.0 ± 1.3	1.21	**23**	35.1 ± 1.0	1.45
8	29.2 ± 1.1	1.57	**24**	56.2 ± 1.2	2.61
9	5.4 ± 0.1	1.35	**25**	21.7 ± 1.2	2.48
10	33.3 ± 1.1	2.10	**26**	34.8 ± 1.0	0.77
11	31.1 ± 1.2	1.97	**27**	19.3 ± 0.8	1.31
12	28.0 ± 1.1	2.63	**28**	49.5 ± 1.2	1.00
13	9.4 ± 0.9	3.16	**29**	17.2 ± 0.9	1.29
14	25.8 ± 1.1	1.10	**30**	0.59 ± 0.04	1.62
15	61.9 ± 1.2	1.43	**31**	2.3 ± 0.5	1.62
16	13.1 ± 1.1	1.99			

[a] IC_{50} values were the mean of quadruplicate of each of two independent experiments. [b]CLog*P* values were calculated by a fragment-based method.[34] cmpd, compound.

Evaluations of 1, 9, 17, 21, 30 on Anti-Tau Hyperphosphorylation Mediated by GSK-3β. Compounds **9**, **17**, **21** and **30** were selected for further evaluation on their effect against GSK-3β mediated tau hyperphosphorylation relative to **1**, as they are the most potent GSK-3β inhibitors within each of the aliphatic, alicyclic, aromatic and fluorinated amide analogues, respectively. We recently established an *in vitro* GSK-3β assay using a whole-cell lysate of human SH-SY5Y

neuroblastomas and demonstrated that the pS396 site on tau protein is GSK-3β specific.[23] Direct GSK-3β inhibition by isoorientin **1** led to its consequent effect against GSK-3β mediated tau hyperphosphorylation on the pS396 site in an *ex vivo* protein matrix of the SH-SY5Y lysate.[23] In analogy, an aliquot of lysate was fortified with GSK-3β (wt/wt 0.25%), and incubated with **9**, **17**, **21**, or **30** at different concentrations (2, 10, and 50 μM) for 2 h followed by an enzyme linked immunosorbent assay (ELISA) with an anti-tau pS396 antibody. TDZD-8 (10 μM) and **1** (100 μM) were used as reference controls. Quantitative ELISA measurements substantiated that introducing exogenous GSK-3β significantly increased phosphorylation by approximately 2.5-fold ($p < 0.0001$) at the site pS396 on tau proteins as compared to their basal levels (lysate fortified with heat-inactivated GSK-3β) (Figure 3). In contrast, treatment of **9**, **17**, **21**, or **30** effectively attenuated tau hyperphosphorylation in a dose-dependent manner ($p < 0.0001$). All four analogues showed vast improvements of anti-tau hyperphosphorylation in comparison to the natural product **1**. Compound **30** at 10 μM exerted an anti-tau effect comparable to TDZD-8 (a known potent GSK-3β inhibitor, $IC_{50} = 2$ μM) at the same concentration ($p < 0.05$). These results demonstrated that the new 6-*C*-glycosylflavone analogues indeed alleviate tau hyperphosphorylation, of which **30** is the most promising candidate suitable for further *in vivo* pharmacological assessments.

GSK-3β Kinetic Studies on the Inhibition Mode of 30. To determine the GSK-3β inhibitory mechanism, the most potent analogue **30** (Figure 4A) was assayed to competitively replace ATP or the GSK-3β substrate GS2 (a peptide derived from human muscle glycogen synthase). Under a constant concentration of the substrate GS2 (17 μM), ATP concentrations varied from 2 to 50 μM and **30** concentrations varied from 0 to 5 μM. The Lineweaver–Burk plots show a

convergence of intersecting lines on the x-axis, indicating an unaltered Michaelis–Menten constant (K_m) but a reduced GSK-3β activity (increased $1/V_{max}$) when the concentration of **30** increased (Figure 4B(a)). This suggested no competition between ATP and **30**. In the second set of experiments under a constant concentration of ATP (10 μM), substrate GS2 concentrations varied from 8 to 66 μM and **30** concentrations varied from 0 to 5 μM. The Lineweaver–Burk plots show that all lines intersected at the same point on the y-axis, suggesting an unchanged $1/V_{max}$ but an increase of K_m when the concentration of **30** increased (Figure 4B(b)). The data demonstrated that **30** competed with the substrate GS2. The enzyme inhibitory behaviors of **30** are similar to that of the parent compound **1**[23] and therefore confirm that the new analogues are indeed reversible and substrate-competitive inhibitors of GSK-3β.

Kinase Selectivity Profile of 30. It is prudent to evaluate kinase selectivity in the early phases of drug discovery. Compound **30** was screened against a panel of 41 human protein kinases for selectivity relevant to AD and other CNS disorders.[9] **30** at 5 μM showed an overall good selectivity as it effectively inhibited GSK-3β by decreasing 92.3% kinase activity ($p < 0.0001$) in comparison to the control (100% kinase activity), whereas it showed only marginal or weak inhibition against 40 out of 41 kinases in the test panel (Figure 4C). Notably, between the two GSK-3 isoforms (GSK-3α and GSK-3β), **30** at 5 μM displayed a 12.3-fold selectivity to GSK-3β (92.3% inhibition) versus GSK-3α (7.5% inhibition). The exceptional selectivity of **30** to GSK-3β could minimize risk of off-target effects.

Evaluation of 30 on Cytotoxicity and Anti-Amyloid Neurotoxicity. To investigate whether semi-synthetic 6-*C*-glycosylflavone analogues exert neuroprotection against Aβ-induced

neurotoxicity, **30** was assayed in an AD cellular model where $A\beta_{42}$ oligomers were administrated in human SH-SY5Y neuroblastomas.[23, 35] Compound **30** displayed a good tolerability profile similar to **1** as no observable cytotoxicity up to a dose of 1000 μM (Figure 5A).[23] On the other hand, treatment of 10 μM $A\beta_{42}$ oligomers decreased cell viability to 40% compared with the controls (Figure 5B). However, such $A\beta_{42}$ neurotoxicity was greatly relieved, as pretreatment of SH-SY5Y cells with **30** at concentrations from 1.25 to 20 μM for 1 h followed by co-incubation with 10 μM $A\beta_{42}$ for 72 h recovered cell viability from 40% to 100% in a dose-dependent manner. The neuroprotective potency of **30** (EC_{50}, 8.7 μM) (Figure 5C) was a 5.4-fold increase in comparison to its parent compound **1** (EC_{50}, 47 μM).[23]

Morphological observations also illustrated that pretreatment by **30** at 10 μM effectively protected the SH-SY5Y cells from $A\beta_{42}$ intoxication, as the neuronal cells were healthy and well differentiated with extended axons and dendrites (Figure 5D). Although a similar neuroprotective activity was observed to **1**, **30** exhibited approximately 20-fold improvement of effectiveness in comparison to its parent compound (effective dose: **30** in 10 μM versus **1** in 200 μM).[23] In a good agreement with our previous findings, **30** and the other 6-*C*-glycosylflavone analogues exerted anti-Aβ neurotoxicity through protecting neurite outgrowth and neuronal differentiation, whose functions are constitutively regulated by GSK-3β and tau protein within axonal microtubules.[7]

Evaluations of 1, 4, 9, 17, 21, 30 on Passive Membrane Permeability. Oral administration is noninvasive and is preferred for chronical diseases such as AD and other CNS disorders. It is advantageous to discover passive membrane permeable AD drugs targeting GSK-3β upon oral administration. The parallel artificial membrane permeability assay (PAMPA) is used to assess

passive and transcellular permeability, which is well correlated with *in vivo* oral absorption rates for drugs that cross the gastrointestinal barrier.[36] In the PAMPA model, the amount of target compounds diffused from a donor compartment to an acceptor compartment through a tri-layer phospholipid pre-coated membrane was measured to assess oral-absorption potential of drug candidates. In the present study, **1**, **4**, **9**, **17**, **21** and **30** were evaluated with the PAMPA assay. Theophylline and atenolol known for their low permeability were used as negative controls. Desipramine known for its high permeability was used as a positive control. The measured P_e values were compared with the literature data.[36]

The new analogues **9**, **17**, **21** and **30** demonstrated a significant increase of permeability upon 5 h of incubation in comparison with their parent compound **1** (Table 3). Methylation of phenolic hydroxyls and transformation of the primary hydroxyl to hydrophobic amides on the *C*-glycone of **1** increased the PAMPA permeability (P_e) ranging from 2.6 to 4.4-fold relative to **1**. Such P_e changes agreed well with the CLog*P* changes (Table 3). The best PAMPA permeability of **30** is probably attributed to the CF_3 group. Multiple hydroxyl groups in *C*-glycone and flavone moieties make **1** poorly permeable, which is consistent with the literature reports.[37] For comparison, luteolin (**4**), an aglycone flavone, had a medium PAMPA permeability similar to **9**, **17**, and **21**, indicating the liability of the polar *C*-glycone of **1** in respect to passive diffusion. Regardless, it is indispensable to assess pharmacokinetics of the new GSK-3β inhibitors for their *in vivo* bioavailability which involves the complexity of active and facilitated transports in addition to passive diffusion.

Table 3. PAMPA Permeability and CLog*P* Values of Compounds Tested

cmpd no.	PAMPA Permeability			CLog*P*
	P_e ($\times 10^{-6}$ cm/s) [a]	*R* (%) [b]	Permeability classification [c]	
Isoorientin (**1**)	0.51 ± 0.01	48	low	0.21
Luteolin (**4**)	1.42 ± 0.07	43	medium	2.31
9	1.55 ± 0.06	46	high	1.35
17	1.77 ± 0.07	20	high	2.55
21	1.35 ± 0.08	30	medium	2.34
30	2.23 ± 0.21	30	high	1.62
Theophylline	0.04 ± 0.01	n/a	low	-0.03
Atenolol [d]	0.29 ± 0.09	40	low	-0.11
Desipramine [d]	13.43 ± 0.91	96	high	4.47

[a] P_e values were the mean of PAMPA measurements (n = 3-4) with ± SD. [b] Percent recovery (*R*%) measures mass retention of compounds trapped inside the PAMPA membrane. [c] PAMPA permeability classification: high ($P_e > 1.5 \times 10^{-6}$ cm/s), medium (1.0×10^{-6} cm/s $\leq P_e \leq 1.5 \times 10^{-6}$ cm/s), low ($P_e < 1.0 \times 10^{-6}$ cm/s). [d] The measured P_e values are comparable to the data in ref.[36]

Computational Modeling

Key Molecular Interactions between New *C*-Glycosylflavones and the Substrate Site of GSK-3β. To elucidate the molecular mechanisms by which the new 6-*C*-glycosylflavones increase the binding affinity and selectivity to GSK-3β relative to **1**, compounds **5-31** were docked into GSK-3β enzyme. The AutoDock Vina program was used in the present study because it has shown good accuracies for binding pose prediction and scoring function.[38-40] This docking tool has been widely used in drug design and applied in many cases of GSK-3β inhibitor discovery.[17, 41]

Two X-ray crystallographic structures of GSK-3β (PDB codes 1PYX[42] and 1H8F[43]) were chosen to take into account for potential induced fit effects upon ligand binding. The GSK-3β in 1PYX contains two Mg^{2+} ions and a ligand ANP, a non-hydrolyzed ATP derivative, at the ATP site. Upon binding of Mg^{2+} ions and an ATP-mimic ligand, it is postulated that GSK-3β undergoes subtle conformational changes in both the ATP and substrate sites for an optimal kinase reaction, a phenomenon known as induced fit effects.[44-45] The GSK-3β structure in 1PYX hence adopts a conformation that resembles the native enzyme ready for substrate recognition. Docking **5-31** into the substrate site of GSK-3β using 1PYX would give more reliable binding poses. On the other hand, the GSK-3β in 1H8F is by far the only available X-ray crystallographic structure containing the ligand HEPES in the substrate site. HEPES in 1H8F may cause induced fit changes of GSK-3β conformation, particularly for the substrate site. Given the new 6-*C*-glycosylflavones are substrate competitive, we used 1PYX and 1H8F in molecular docking. The docking method was validated by re-docking and cross-docking experiments using both ATP-competitive and substrate-competitive inhibitors (Supporting Information S1).

The synthetic 6-*C*-glycosylflavones (**5-31**) and their parent **1** were thus docked into 1PYX and 1H8F. Docking scores of 1PYX show a better linear fit to the experimental pIC50 values (R^2 = 0.7844) than that of 1H8F (R^2 = 0.6999), suggesting more accurate predictions of binding poses using 1PYX than 1H8F (Supporting Information S2). The 1PYX docking dataset was therefore used in the remainder of the study to analyze the molecular interactions responsible for the improved potency and selectivity to GSK-3β.

The docking results of 1PYX showed that the *C*-glycone moiety of **5-31** forms hydrogen bonds with GSK-3β residues Gln89, Asn95, Arg96 and Glu97 within the substrate pocket, which is similar to **1** (Supporting Information S3). Moreover, the newly introduced hydrophobic groups

indeed exhibit a favorable ligand pose to the concave surface comprised of Phe67, Val87, Leu88 and Phe93 on GSK-3β. The most potent compounds **30** and **31** (IC_{50}, 0.59 and 2.3 μM, respectively) contain a CF_3 moiety, which may form orthogonal multipolar interactions for protein binding.[46-47] To visualize such molecular interactions, we conducted flexible-residue docking[40, 48] to refine binding poses of **9**, **30** and **31** in 1PYX. To prepare GSK-3β structure, side chains of Ser66, Phe67, Leu88, Gln89, Asp90, Phe93, Asn95 and Lys183 within the substrate site were treated flexible. The docking results of **30** suggested formation of orthogonal multipolar interactions. The (*S*)-CF_3 in **30** shows a favorable geometry within typical F···C distances to Leu88 (backbone amide carbonyl carbon, 3.3 Å), Gln89 (backbone amide carbonyl carbon, 3.6 Å) and Asp90 (side chain carbonyl carbon, 3.3 and 3.8 Å) (Figure 6C). It also forms a polar interaction with the backbone NH of Asp90 (F···H distance, 2.6 Å). In contrast, the (*R*)-CF_3 group of **31** is absent from these interactions probably owing to the orientation and steric hindrance by switching CH_3 and CF_3 positions at the stereocenter (Figures 6B-6C). Therefore, only hydrophobic interactions with Phe67, Val87 and Leu88 of GSK-3β exist in **31** (improper configuration of CF_3 for orthogonal multipolar interactions) as well as **9** (lack of CF_3) (Figures 6A-6B).

Interestingly, the docking results showed that the catechol B-ring of the flavone core in **9**, **30** and **31** appears to have a π-cation interaction with Lys183.[49-50] The distance between the catechol B-ring center and ε–NH_3^+ cation of Lys183 is 4.1 Å at an angle of 71.5° (Figure 6C and Supporting Information S4). In conjunction, the side chain ε–NH_3^+ of Lys183 forms weak hydrogen bonds with two methoxy oxygen atoms of catechol B-ring (distances of 3.1 and 3.2 Å). The orthogonal multipolar and π-cation interactions potentially enhance the binding affinity to GSK-3β.

Potential Causes for the Isoform-Selectivity of 30 between GSK-3α and GSK-3β. Isoform-selectivity of **30** to GSK-3β over GSK-3α (Figure 4C) was assessed with comparative molecular modeling. Yet no X-ray crystallographic structures of GSK-3α available in PDB, a homology model of GSK-3α was built with the SWISS-MODEL server[51] (Supporting Information S5). A full human GSK-3α amino acid sequence (UniProt code: P49840) was searched against protein databases in BLAST and HHblits and overall 4470 templates were found. A GSK-3β template (PDB code 1PYX) resulted in a top ranking with an overall sequence identity of 82.97%, thereby selected for homology modeling of GSK-3α. A sequence alignment between the two GSK-3 isoforms indicated that GSK-3α has extra amino acid portions flanking the N- and C-termini of GSK-3β (Supporting Information S6). Within the matched sequence portion, most amino acid differences occur in the N- and C-terminal regions. In contrast, both the ATP and substrate domains of GSK-3α/β isoforms are conserved as high as 92.37% identical, in which only few amino acid residues are different in these regions. The superposition and comparison of GSK-3β structure (PDB code 1PYX) with the GSK-3α homology model (Figure 7A) implied that those subtle differences of amino acid residues in the kinase catalytic domain (both ATP and substrate pockets) may affect substrate recognition as well as ligand binding. Intriguingly, docking experiment using the GSK-3α homology model showed that **30** resides a similar location in the substrate site in comparison to GSK-3β docking data (Figures 7B-7C). However, the resulting binding pose of **30** in GSK-3α favors neither a π-cation interaction of catechol B-ring nor the orthogonal multipolar interactions of the (*S*)-CF_3 group. It is conceivable that the isoform-selectivity of **30** to GSK-3β might be in part due to the lack of these critical molecular interactions in GSK-3α. Instead, the (*S*)-trifluoroisopropyl group of **30** simply exerts

hydrophobic affinity with the homologous residues Phe130, Val150, and Leu151 in the substrate site of GSK-3α (Figure 7C).

Discussion

GSK-3β plays a central role in signaling pathways of AD. Accumulating evidence has demonstrated that GSK-3β is activated abnormally by Aβ and in turn hyperphosphorylates tau proteins in neurons. This eventually triggers the tauopathic cascade in AD progression.[1, 7-8] Development of GSK-3β inhibitors as a disease-modifying therapy for AD, therefore, is highly attractive. In recent years, discovery of selective inhibitors targeting the substrate site of GSK-3β has emerged as a rational and feasible strategy in AD drug design.[11] Unlike the ATP-site directed GSK-3β inhibitors that frequently bind to many off-target kinases, inhibitors targeting the substrate site on GSK-3β plausibly overcome this limitation. GSK-3β phosphorylates its specific substrates for biological processes such as glucose homeostasis, immune response, neurogenesis, cell proliferation and apoptosis, and circadian rhythm, which has a plethora of normal functions for human health.[52] However, GSK-3β is aberrantly overactive in AD. Subtle modulation of GSK-3β activity at a normal level rather than complete shut-off to prevent disruption of its normal cellular functions will be highly appreciated in AD therapy.[8] Targeting the substrate site to intervene the GSK-3β-substrate recognition would be a feasible means to find selective inhibitors.[14] Until now, substrate-competitive inhibitors of GSK-3β are limited in the structural classes of marine alkaloid manzamines,[15] labdane diterpenoid andrographolide,[17] peptidomimetic inhibitors,[18] and synthetic compound ITDZ series.[16] These inhibitors were in the low micromolar to sub-micromolar range of potency, but exhibited a good selectivity to GSK-3β under *in vitro* or *in vivo* evaluations. Such findings substantiate the rationale of developing substrate-competitive

inhibitors of GSK-3β for AD by which the agents can attain an utmost therapeutic advantage – a high selectivity to avoid potential side effects.

Herein, we reported a new structural class of substrate-competitive inhibitors of GSK-3β, inspired by isoorientin (**1**), containing a 6-*C*-glycosylflavone scaffold. It is a valuable addition to the known substrate-competitive inhibitors and offers new lead compounds for AD. The inhibitors are new chemical probes allowing to elucidate the underling mechanisms of GSK-3β inhibition and selectivity.

The SAR analysis, *in vitro* enzymatic kinetics, and *in silico* docking studies indicate that both the presence and position of *C*-glycone on the flavone core are essential features binding to the substrate site on GSK-3β. A flavone core (**4**) alone is promiscuous and tends to sneak in the ATP site and thus lose the required selectivity (Supporting Information S1). The presence of a *C*-glycone at 8-position (**3**, IC_{50}, > 5 mM) rather than 6-position (**1**, IC_{50}, 185 μM) results in an unfavorable binding pose to the substrate site plausibly due to the loss of key hydrogen bonds with Gln89, Asp90, Asn95, and Arg96 (Supporting Information S3). Such unique SAR features inspired us to semi-synthesize a series of novel analogues of **1** that selectively inhibit GSK-3β at the substrate site. Data suggest that the new lipophilic amide analogues (**8-31**) increase the potency against GSK-3β for 3–310 fold (Table 2) and passive membrane permeability for 2.6–4.4 fold relative to **1** (Table 3). Systematic modifications of the carbon-chain length and ring size and bioisosteric replacement in the R_2-group on the *C*-glycone of **1** (Table 1) confer a dramatic GSK-3β potency improvement. The structural modifications contribute hydrophobic affinities with Phe67, Val87 and Leu88 in the substrate site of GSK-3β (Supporting Information S3), which is concurrently supported by the LiPE analysis (LiPE highlights potency changes to the net of lipophilicity). Compounds **9**, **30**, and **31** containing an isopropyl moiety have IC_{50} values

of 5.4, 0.59, and 2.3 μM, respectively, which are most potent among the analogues. It suggests that they adopt a suitable carbon-chain length and topological size within the hydrophobic cleft of the substrate site. LiPE analysis also indicates that **9**, **30**, and **31** are quality ligands (LiPE values ≥ 4, Figure 2B). In addition, the new analogues alleviate tau hyperphosphorylation and Aβ neurotoxicity through GSK-3β inhibition in the human SH-SY5Y neuronal model of AD (Figures 3 and 5).

With respect to the GSK-3β selectivity of **30**, π-cation interaction and orthogonal multipolar interactions appear to play a critical role. In protein structures, the aromatic side chain of Phe or Tyr usually involves a favorable π-cation interaction with the cationic side chain of Lys or Arg.[49] In analogy, if a small aromatic ligand binds to a protein, potential π-cation interactions would be an important contribution to the binding affinity. Such phenomena have been exemplified in our previous study[50] as well as other investigations.[53-54] Flavonoids seem to be the case – interactions between the aromatic A/B-rings with the cationic Lys or Arg residues.[41, 55] In the docking experiments, we found that the catechol B-ring of the flavone core in **30** forms a π-cation interaction with Lys183 of GSK-3β (distance, 4.1 Å; angle, 71.5°). To a certain extent, this might stabilize the binding conformation and orientation within the substrate site.

It is known that a fluorine atom has distinct chemical properties contributing to the molecular recognition.[46] Fluorinated compounds commonly form orthogonal multipolar interactions with the backbone and side chain carbonyl carbons (Asp/Glu/Asn/Gln) or the guanidinium carbon (Arg) of amino acid residues in protein structures.[46-47] Introduction of a CF_3 group is a common tactic in drug design. It is estimated that substitution of CH_3 for CF_3 may improve 5- to 10-fold ligand binding affinity.[47, 56] In the present study, **27** (IC_{50}, 19.3 μM) and **29** (IC_{50}, 17.2 μM) containing a 2,2,2-trifluoroethyl and 3,3,3-trifluoropropyl, respectively, show an improved

potency relative to their analogue **8** (IC_{50}, 29.2 μM) without a CF_3 group. In addition, **30** and **31** containing a 1,1,1-trifluoroisopropyl are more potent than their analogue **9** without a CF_3 group. Docking experiments suggest that the isopropyl (*S*)-CF_3 group of **30** interacts with the backbone and side chain carbonyls of Leu88, Gln89, and Asp90 (Figure 6C) within typical interaction distances (F···C, 3.0–3.7 Å).[47] Such orthogonal multipolar interactions might in part give rise to an increased potency of **30** (IC_{50}, 0.59 μM) against GSK-3β approximately 9-fold and 4-fold compared to **9** (IC_{50}, 5.4 μM) and **31** (IC_{50}, 2.3 μM), respectively. Conversely, **31** with a (*R*)-CF_3 group may be lacking these critical molecular interactions (Figures 6B-6C) and thus has weaker binding affinity than **30**. The differential and stereospecific binding of the CF_3 group between **30** and **31** plausibly explains the high inhibitory selectivity to GSK-3β (Figures 2 and 4).

Interestingly, **30** exhibits isoform-selectivity to GSK-3β over GSK-3α, which deserves discussion. In humans, GSK-3α (51 kDa) and GSK-3β (47 kDa) are derived from different genes and have distinct functions.[52] Both isoforms share an overall sequence identity of 83%, especially at the ATP catalytic domain with 93% identity.[57] However, they differ substantially in the N- and C-terminal lobes that are thought to cause protein conformational dynamics and differential cellular localization.[52, 57] Subtle amino acid differences in the substrate site between two isoforms (Supporting Information S6) putatively affect substrate recognition and preference as noted in the literature.[58-59] Wang et al. reported that GSK-3β phosphorylates a substrate (phosphatase inhibitor-2) 10-time faster than GSK-3α,[58] indicating the differential substrate recognition of GSK-3 isoforms. Soutar et al. demonstrated that the specific sites T231, T235, and S396 on tau proteins are solely phosphorylated by GSK-3β but not GSK-3α,[59] giving an evidence of substrate specificity between two isoforms. Those studies pose a possibility to discover isoform-selective inhibitors via targeting the substrate site of GSK-3β. Compound **30** attains

GSK-3β isoform-selectivity probably because of both the π-cation interaction with Lys183 and the orthogonal multipolar interactions with Leu88, Gln89, and Asp90 in GSK-3β on the basis of the comparative docking of GSK-3α/β (Figures 6C and 7). In contrast, **30** is absent from those key molecular interactions within the substrate site of GSK-3α (Figure 7C). In addition, the highly non-conserved regions in GSK-3α, such as the N- and C-terminal domains (Figure 7A), can modulate enzyme conformations and thereby may affect the binding of **30**. Notwithstanding, the molecular mechanism suggested by computational modeling requires further verification by conclusive experimental evidence.

Conclusions

In summary, we described a new class of substrate-competitive inhibitors of GSK-3β focusing on modifications of the primary hydroxyl group in the *C*-glycone of isoorientin (**1**). The results demonstrated that the 6-*C*-glycone moiety of the new inhibitors defines the specific binding at the substrate site rather than the ATP site on GSK-3β. The data also help explore topological requirements in the substrate site of GSK-3β and highlight the critical SAR. Those inhibitors effectively attenuate tau hyperphosphorylation and amyloid neurotoxicity in molecular and cellular AD models by which the mechanism is involved in GSK-3β inhibition via a non-ATP competitive but substrate competitive manner. The inhibitors not only significantly increased the potency, kinase selectivity, and isoform-selectivity, but also improved passive membrane permeability in comparison with the natural product counterparts. Among them, **30** (IC_{50}, 0.59 μM) showed a potency improvement by 310-fold and a promising profile in various biological assessments, which warrants further exploration. SAR analyses and *in silico* mechanistic investigations suggested that the hydrophobic, π-cation and orthogonal multipolar interactions of

30 with the substrate site lead to selective inhibition against GSK-3β, but neither GSK-3α nor a broad panel of kinases tested. Nevertheless, additional SAR knowledge and physiochemical property optimization of the GSK-3β inhibitors based on the 6-*C*-glycosylflavone scaffold are essential to the CNS drug discovery campaign. Pharmacokinetics and *in vivo* animal studies of the new GSK-3β inhibitors will help understand drug delivery, target engagement and efficacy, which would suggest the therapeutic potential of these agents for AD and other GSK-3β relevant neuropsychiatric and neurodegenerative diseases.

Methods

Chemicals and Reagents. All solvents and reagents were from commercial sources and were used without further purification. Natural flavones (isoorientin, orientin, isovitexin, and luteolin), staurosporine, TDZD-8, theophylline, atenolol, desipramine, $TMSCHN_2$, $[TEMPO]^+[BF_4]^-$, HCTU, organic amines, and protease inhibitor cocktail were from Sigma-Aldrich (Saint Louis, MO). β-Amyloid fragment peptide 1-42 ($A\beta_{42}$) was from AnaSpec (Fremont, CA). Kinase Selectivity Profiling Assay Kit, ADP-Glo Kinase Assay Kit, and CellTiter 96 AQueous One Solution Cell Proliferation MTX Assay Kit were from Promega (Madison, WI). Human Tau pS396 ELISA Kit and Cell Extraction Buffer were from Invitrogen (Camarillo, CA). Pre-coated PAMPA plate system was from Corning (Tewksbury, MA).

General Experimental Procedures. High-resolution mass spectrometric data were obtained on a Bruker maXis Impact nanoLC-QTOF-MS spectrometer in ESI positive mode. Accurate masses of all analytes were obtained from the pseudo-molecule $[M+H]^+$ and were within 5 ppm mass error. ^1H, ^{13}C and 2D NMR data were recorded with a Varian Unity Inova 500 MHz spectrometer. NMR spectra were referenced to the appropriate residual solvent signal (δ_H 2.50,

δ_C 39.5 for DMSO-d_6) with chemical shifts reported in δ units (ppm). Resonance multiplicities are denoted s, d, t, q, m, and br for singlet, doublet, triplet, quartet, multiplet, and broad, respectively.

All reactions were monitored by LC-MS (Bruker nanoLC-QTOF-MS). Compounds in crude reaction mixtures were separated by flash column chromatography on HyperSep C18 (40–63 μm), and purified by semi-preparative reverse phase Agilent HPLC with a diode array detector (Waters XSELECT CSH Phenyl-Hexyl column, 150 × 10 mm, 5 μm, a linear gradient over 30 min from 10 to 50% aqueous acetonitrile containing 0.1% formic acid, flow rate 2.5 mL/min).

The purity of each compound was determined by analytical reverse phase Agilent HPLC with a diode array detector (Waters XSELECT CSH Fluoro-Phenyl column, 150 × 4.6 mm, 3.5 μm, isocratic elution with 35% aqueous acetonitrile containing 0.1% formic acid, detection at 210, 254, and 340 nm, flow rate of 0.8 mL/min). All the tested compounds were over 95% purity by HPLC-UV at 210, 254, and 340 nm.

Luminescent measurement was performed on an Agilent Cary Eclipse fluorescence spectrophotometer. Optical absorbance was measured on a Multiskan GO Microplate spectrophotometer. Microscopic images were observed under a Nikon Diaphot inverted tissue culture microscope with Optronics MicroFire microscope camera.

General Procedure for the Semi-Synthesis of *C*-Glycosylflavone Analogues.

Preparation of Compound 5. The chemoselective methylation proceeded as described.[28] To a stirred solution of **1** (45 mg, 0.1 mmol) in a mixture of toluene (6 mL) and methanol (4 mL) was added $TMSCHN_2$ (2 M in hexane, 0.5 mL, 1 mmol). The reaction solution was stirred at room temperature for 8 h and the solvent was evaporated. The residue was purified by RP-HPLC (Waters XSELECT CSH Fluoro-Phenyl column, 150 × 4.6 mm, 3.5 μm, isocratic elution with

35% aqueous acetonitrile containing 0.1% formic acid, detection at 210, 254, and 340 nm, flow rate of 0.8 mL/min) to afford **5**.

2-(3,4-Dimethoxyphenyl)-5,7-dimethoxy-6-((2*S*,3*R*,4*R*,5*S*,6*R*)-3,4,5-trihydroxy-6-(hydroxymethyl)tetrahydro-2*H*-pyran-2-yl)-4*H*-chromen-4-one (5). Light yellow solid (80% yield). ^{1}H NMR (DMSO-d_6) δ 7.65 (dd, J = 8.6, 2.2 Hz, 1H), 7.54 (d, J = 2.2 Hz, 1H), 7.12 (d, J = 8.6 Hz, 1H), 7.09 (br s, 1H), 6.72 (br s, 1H), 4.65 (br d, J = 9.7 Hz, 1H), 4.05 (dd, J = 12.7, 9.2 Hz, 1H), 3.89 (s, 3H), 3.86 (s, 3H), 3.81 (s, 3H), 3.77 (s, 3H), 3.72 (dd, J = 12.6, 12.5 Hz, 1H), 3.34 – 3.28 (m, 1H), 3.27 – 3.12 (m, 3H). ^{13}C NMR (DMSO-d_6) δ 175.5, 163.4, 160.2, 158.9, 158.5, 151.8, 149.1, 123.2, 119.7, 111.9, 111.3, 109.4, 107.1, 107.0, 97.0, 82.0, 79.2, 73.1, 71.3, 70.9, 62.6, 62.0, 61.8, 56.4, 55.8. HRESI-TOFMS *m/z* $[M+H]^+$ 505.1710 (calcd for $C_{25}H_{29}O_{11}^+$, 505.1704, -1.1 ppm error). HPLC purity: 97.1% (210 nm).

Preparation of Compound 6. To a stirred solution of **5** (45 mg, 0.09 mmol) in a mixture of dichloromethane (6 mL) and pyridine (3 mL) was added $[TEMPO]^+[BF_4]^-$ (oxoammonium salt, 60 mg, 0.2 mmol). The reaction mixture was stirred at room temperature for 5 h. The reaction was quenched by adding drops of methanol and then evaporated to dryness. The residue was reconstituted in 5% MeOH/H_2O and then eluted on a HyperSep C18 column using the same solvents to remove the red-orange nitroxide. Elution was continued with 90% MeOH/H_2O and the eluate was collected as the crude product, which was further purified by RP-HPLC (Waters XSELECT CSH Fluoro-Phenyl column, 150 × 4.6 mm, 3.5 μm, isocratic elution with 35% aqueous acetonitrile containing 0.1% formic acid, detection at 210, 254, and 340 nm, flow rate of 0.8 mL/min) to afford **6**.

(2*S*,3*S*,4*R*,5*R*,6*S*)-6-(2-(3,4-Dimethoxyphenyl)-5,7-dimethoxy-4-oxo-4*H*-chromen-6-yl)-3,4,5-trihydroxytetrahydro-2*H*-pyran-2-carboxylic acid (6). Light yellow solid (95% yield). ^{1}H NMR (DMSO-d_6) δ 7.65 (dd, J = 8.5, 2.0 Hz, 1H), 7.54 (d, J = 2.0 Hz, 1H), 7.12 (d, J = 8.5 Hz, 1H), 7.09 (br s, 1H), 6.76 (d, J = 6.6 Hz, 1H), 4.60 (d, J = 10.1 Hz, 1H), 4.02 (m, 1H), 3.89 (s, 3H), 3.85 (s, 3H), 3.82 (s, 3H), 3.75 (s, 3H), 3.30 – 3.16 (m, 3H). ^{13}C NMR (DMSO-d_6) δ 175.5, 173.0, 162.2, 160.4, 158.9, 158.5, 151.9, 149.2, 123.2, 119.7, 111.9, 111.4, 109.4, 107.1, 107.0, 97.1, 79.0, 78.5, 74.1, 72.5, 71.3, 63.5, 62.6, 56.6, 56.1. HRESI-TOFMS *m/z* $[M+H]^+$ 519.1502 (calcd for $C_{25}H_{27}O_{12}^+$, 519.1497, -0.9 ppm error). HPLC purity: 97.8% (210 nm).

Preparation of Compound 7. To a stirred solution of **6** (1 mg, 2 μmol) in a mixture of toluene (1.5 mL) and methanol (1 mL) was added $TMSCHN_2$ (2 M in hexane, 2 μL, 4 μmol). The reaction solution was stirred at room temperature for 1 h and the solvent was evaporated. The residue was purified by RP-HPLC (Waters XSELECT CSH Fluoro-Phenyl column, 150 × 4.6 mm, 3.5 μm, isocratic elution with 35% aqueous acetonitrile containing 0.1% formic acid, detection at 210, 254, and 340 nm, flow rate of 0.8 mL/min) to afford **7**.

Methyl (2*S*,3*S*,4*R*,5*R*,6*S*)-6-(2-(3,4-dimethoxyphenyl)-5,7-dimethoxy-4-oxo-4*H*-chromen-6-yl)-3,4,5-trihydroxytetrahydro-2*H*-pyran-2-carboxylate (7). Light yellow solid (87% yield). ^{1}H NMR (DMSO-d_6) δ 7.69 (dd, J = 8.5, 2.1 Hz, 1H), 7.56 (d, J = 2.1 Hz, 1H), 7.15 (br s, 1H), 7.12 (d, J = 8.5 Hz, 1H), 6.80 (d, J = 5.5 Hz, 1H), 4.57 (d, J = 9.6 Hz, 1H), 4.00 (m, 1H), 3.89 (s, 3H), 3.85 (s, 3H), 3.80 (s, 3H), 3.73 (s, 3H), 3.63 (s, 3H), 3.29 – 3.13 (m, 3H). ^{13}C NMR (DMSO-d_6) δ 175.6, 172.9, 162.1, 160.1, 159.0, 158.4, 151.8, 149.1, 123.2, 119.7, 111.9, 111.4, 109.4, 107.1, 107.0, 97.0, 79.0, 78.5, 74.1, 72.5, 71.3, 63.4, 62.6, 56.6, 56.0, 51.8. HRESI-TOFMS *m/z* $[M+H]^+$ 533.1656 (calcd for $C_{26}H_{29}O_{12}^+$, 533.1654, -0.5 ppm error). HPLC purity: 97.1% (210 nm).

Preparation of Compounds 8-31. To a stirred solution of **6** (5 mg, 9.7 μmol) in a mixture of dimethylformamide (1 mL) and DIPEA (0.5 mL) was added HCTU (10 mg, 24 μmol) and then stirred for 10 min at room temperature. To this solution was added corresponding organic amines (each 50 μmol) and stirred at room temperature for 5 h.

The reaction was quenched by adding 1 *N* HCl followed by evaporation of solvents to dryness. The residue was purified by RP-HPLC (Waters XSELECT CSH Fluoro-Phenyl column, 150 × 4.6 mm, 3.5 μm, isocratic elution with 35% aqueous acetonitrile containing 0.1% formic acid, detection at 210, 254, and 340 nm, flow rate of 0.8 mL/min) to afford the final products.

(2*S*,3*S*,4*R*,5*R*,6*S*)-6-(2-(3,4-Dimethoxyphenyl)-5,7-dimethoxy-4-oxo-4*H*-chromen-6-yl)-3,4,5-trihydroxy-*N*-propyltetrahydro-2*H*-pyran-2-carboxamide (8). Light yellow solid (90% yield). ^{1}H NMR (DMSO-d_6) δ 7.67 (d, J = 8.7 Hz, 1H), 7.53 (d, J = 2.2 Hz, 1H), 7.13 (s, 1H), 7.12 (d, J = 8.7 Hz, 1H), 6.76 (d, J = 5.9 Hz, 1H), 4.67 (br d, J = 10.1 Hz, 1H), 4.06 (q, J = 10.3 Hz, 1H), 3.87 (s, 3H), 3.83 (s, 3H), 3.77 (s, 3H), 3.71 (s, 3H), 3.60 (m, 1H), 3.50 (m, 1H), 3.23 (m, 1H), 2.99 (m, 2H), 1.36 (m, 2H), 0.78 (td, J = 7.4, 2.2 Hz, 3H). ^{13}C NMR (DMSO-d_6) δ 175.7, 168.7, 163.4, 160.5, 160.2, 158.4, 151.6, 149.3, 123.1, 120.4, 112.2, 111.9, 109.6, 107.2, 107.0, 96.8, 80.6, 79.0, 74.4, 71.6, 69.6, 63.9, 63.1, 56.7, 56.1, 40.8, 22.6, 11.5. HRESI-TOFMS *m/z* $[M+H]^+$ 560.2135 (calcd for $C_{28}H_{34}NO_{11}^+$, 560.2126, -1.6 ppm error). HPLC purity: 98.6% (210 nm).

(2*S*,3*S*,4*R*,5*R*,6*S*)-6-(2-(3,4-Dimethoxyphenyl)-5,7-dimethoxy-4-oxo-4*H*-chromen-6-yl)-3,4,5-trihydroxy-*N*-isopropyltetrahydro-2*H*-pyran-2-carboxamide (9). Light yellow solid (90% yield). ^{1}H NMR (DMSO-d_6) δ 7.67 (d, J = 8.1 Hz, 1H), 7.55 (d, J = 2.2 Hz, 1H), 7.14 (br s, 1H), 7.12 (d, J = 9.7 Hz, 1H), 6.77 (d, J = 5.1 Hz, 1H), 4.67 (d, J = 9.7 Hz, 1H), 4.05 (m, 1H),

3.92 (s, 3H), 3.89 (s, 3H), 3.85 (s, 3H), 3.83 (m, 1H), 3.81 (s, 3H), 3.59 (m, 1H), 3.57 (m, 1H), 3.23 (m, 1H), 1.04 (d, J = 6.4 Hz, 3H), 1.01 (d, J = 6.8 Hz, 3H). ^{13}C NMR (DMSO-d_6) δ 175.5, 168.7, 163.3, 161.7, 160.1, 158.7, 152.1, 149.2, 123.1, 119.5, 111.9, 111.3, 109.4, 107.1, 107.0, 97.0, 79.8, 78.5, 73.8, 71.4, 70.3, 63.4, 62.5, 56.6, 55.8, 40.3, 22.2, 22.2. HRESI-TOFMS *m/z* $[M+H]^+$ 560.2117 (calcd for $C_{28}H_{34}NO_{11}^+$, 560.2126, 1.7 ppm error). HPLC purity: 97.2% (210 nm).

(2*S*,3*S*,4*R*,5*R*,6*S*)-6-(2-(3,4-Dimethoxyphenyl)-5,7-dimethoxy-4-oxo-4*H*-chromen-6-yl)-3,4,5-trihydroxy-*N*-butyltetrahydro-2*H*-pyran-2-carboxamide (10). Light yellow solid (90% yield). ^{1}H NMR (DMSO-d_6) δ 7.68 (d, J = 8.6 Hz, 1H), 7.55 (d, J = 2.2 Hz, 1H), 7.14 (s, 1H), 7.12 (d, J = 8.6 Hz, 1H), 6.81 (d, J = 6.7 Hz, 1H), 4.67 (br d, J = 10.2 Hz, 1H), 4.06 (m, 1H), 3.89 (s, 3H), 3.85 (s, 3H), 3.80 (s, 3H), 3.74 (s, 3H), 3.58 (m, 1H), 3.50 (m, 1H), 3.23 (m, 1H), 3.02 (m, 2H), 1.34 (m, 2H), 1.23 (m, 2H), 0.83 (m, 3H). ^{13}C NMR (DMSO-d_6) δ 175.9, 168.8, 163.2, 160.3, 160.2, 158.3, 151.8, 149.1, 123.3, 119.7, 111.7, 111.5, 109.2, 107.2, 106.9, 96.5, 80.1, 78.8, 74.0, 71.5, 70.3, 63.8, 62.9, 56.7, 56.1, 38.2, 31.2, 19.6, 13.8. HRESI-TOFMS *m/z* $[M+H]^+$ 574.2289 (calcd for $C_{29}H_{36}NO_{11}^+$, 574.2283, -1.1 ppm error). HPLC purity: 97.4% (210 nm).

(2*S*,3*S*,4*R*,5*R*,6*S*)-6-(2-(3,4-Dimethoxyphenyl)-5,7-dimethoxy-4-oxo-4*H*-chromen-6-yl)-3,4,5-trihydroxy-*N*-isobutyltetrahydro-2*H*-pyran-2-carboxamide (11). Light yellow solid (88% yield). ^{1}H NMR (DMSO-d_6) δ 7.62 (d, J = 8.8 Hz, 1H), 7.49 (d, J = 1.9 Hz, 1H), 7.14 (s, 1H), 7.11 (d, J = 8.6 Hz, 1H), 6.81 (d, J = 6.9 Hz, 1H), 4.68 (br d, J = 10.2 Hz, 1H), 4.07 (m, 1H), 3.89 (s, 3H), 3.84 (s, 3H), 3.80 (s, 3H), 3.75 (s, 3H), 3.62 (m, 1H), 3.49 (m, 1H), 3.24 (m, 1H), 2.87 (t, J = 6.4 Hz, 2H), 1.66 (m, 1H), 0.79 (d, J = 6.7 Hz, 6H). ^{13}C NMR (DMSO-d_6) δ 176.2, 167.3, 163.5, 160.6, 160.7, 158.8, 153.1, 149.5, 123.7, 120.7, 113.0, 112.7, 112.4, 108.3,

107.4, 97.7, 81.0, 79.9, 75.2, 72.8, 71.5, 64.6, 64.1, 57.8, 56.9, 47.2, 29.4, 21.3, 21.3. HRESI-TOFMS *m/z* $[M+H]^+$ 574.2292 (calcd for $C_{29}H_{36}NO_{11}^+$, 574.2283, -1.6 ppm error). HPLC purity: 99.1% (210 nm).

(2*S*,3*S*,4*R*,5*R*,6*S*)-6-(2-(3,4-Dimethoxyphenyl)-5,7-dimethoxy-4-oxo-4*H*-chromen-6-yl)-3,4,5-trihydroxy-*N*-pentyltetrahydro-2*H*-pyran-2-carboxamide (12). Light yellow solid (89% yield). ^{1}H NMR (500 MHz, DMSO-d_6) δ 7.68 (d, J = 8.6 Hz, 1H), 7.55 (d, J = 2.1 Hz, 1H), 7.14 (s, 1H), 7.12 (d, J = 8.6 Hz, 1H), 6.81 (d, J = 6.3 Hz, 1H), 4.67 (br d, J = 10.2 Hz, 1H), 4.06 (m, 1H), 3.89 (s, 3H), 3.85 (s, 3H), 3.80 (s, 3H), 3.74 (s, 3H), 3.58 (m, 1H), 3.50 (m, 1H), 3.22 (m, 1H), 3.03 (m, 2H), 1.35 (m, 2H), 1.23 (m, 2H), 1.20 (m, 2H), 0.83 (m, 3H). ^{13}C NMR (DMSO-d_6) δ 175.9, 168.9, 163.2, 160.5, 160.3, 158.5, 151.9, 149.2, 123.4, 119.7, 111.8, 111.6, 109.3, 107.0, 106.8, 96.4, 80.1, 78.8, 73.5, 71.6, 70.4, 63.5, 62.7, 56.1, 55.9, 38.4, 28.7, 28.6, 21.9, 14.0. HRESI-TOFMS *m/z* $[M+H]^+$ 588.2456 (calcd for $C_{30}H_{38}NO_{11}^+$, 588.2439, -2.8 ppm error). HPLC purity: 98.2% (210 nm).

(2*S*,3*S*,4*R*,5*R*,6*S*)-6-(2-(3,4-Dimethoxyphenyl)-5,7-dimethoxy-4-oxo-4*H*-chromen-6-yl)-3,4,5-trihydroxy-*N*-hexyltetrahydro-2*H*-pyran-2-carboxamide (13). Light yellow solid (90% yield). ^{1}H NMR (DMSO-d_6) δ 7.68 (d, J = 8.6 Hz, 1H), 7.55 (d, J = 2.3 Hz, 1H), 7.14 (s, 1H), 7.12 (d, J = 8.6 Hz, 1H), 6.81 (d, J = 5.9 Hz, 1H), 4.66 (br d, J = 10.5 Hz, 1H), 4.06 (q, J = 8.6 Hz, 1H), 3.89 (s, 3H), 3.84 (s, 3H), 3.80 (s, 3H), 3.74 (s, 3H), 3.60 (m, 1H), 3.50 (m, 1H), 3.23 (m, 1H), 3.01 (m, 2H), 1.40 – 1.15 (m, 8H), 0.82 (m, 3H). ^{13}C NMR (DMSO-d_6) δ 175.6, 168.8, 163.4, 160.3, 160.2, 158.6, 151.8, 149.1, 123.1, 119.6, 112.1, 111.8, 109.3, 107.1, 107.0, 97.1, 79.9, 78.7, 74.5, 71.5, 69.4, 63.5, 62.7, 56.6, 56.0, 38.5, 31.0, 28.9, 26.1, 22.1, 13.9. HRESI-TOFMS *m/z* $[M+H]^+$ 602.2572 (calcd for $C_{31}H_{40}NO_{11}^+$, 602.2596, 3.9 ppm error). HPLC purity: 98.5% (210 nm).

(2*S*,3*S*,4*R*,5*R*,6*S*)-*N*-Cyclopropyl-6-(2-(3,4-dimethoxyphenyl)-5,7-dimethoxy-4-oxo-4*H*-chromen-6-yl)-3,4,5-trihydroxytetrahydro-2*H*-pyran-2-carboxamide (14). Light yellow solid (82% yield). ^{1}H NMR (DMSO-d_6) δ 7.67 (dt, J = 8.3, 2.2 Hz, 1H), 7.54 (d, J = 2.2 Hz, 1H), 7.16 (s, 1H), 7.12 (d, J = 8.3 Hz, 1H), 6.78 (d, J = 5.7 Hz, 1H), 4.64 (br d, J = 9.7 Hz, 1H), 4.06 (q, J = 8.9 Hz, 1H), 3.88 (s, 3H), 3.84 (s, 3H), 3.79 (s, 3H), 3.73 (s, 3H), 3.51 (m, 1H), 3.50 (m, 1H), 3.19 (m, 1H), 2.62 (m, 1H), 0.79 (m, 2H), 0.58 (m, 2H). ^{13}C NMR (DMSO-d_6) δ 175.3, 167.6, 163.4, 161.5, 160.3, 159.6, 152.5, 149.3, 123.4, 119.8, 111.8, 111.5, 109.4, 107.7, 107.0, 97.0, 80.2, 78.9, 74.1, 71.3, 70.3, 63.5, 62.8, 56.1, 55.8, 23.1, 10.8, 10.8. HRESI-TOFMS *m/z* $[M+H]^+$ 558.1967 (calcd for $C_{28}H_{32}NO_{11}^+$, 558.1970, 0.5 ppm error). HPLC purity: 98.2% (210 nm).

(2*S*,3*S*,4*R*,5*R*,6*S*)-*N*-Cyclobutyl-6-(2-(3,4-dimethoxyphenyl)-5,7-dimethoxy-4-oxo-4*H*-chromen-6-yl)-3,4,5-trihydroxytetrahydro-2*H*-pyran-2-carboxamide (15). Light yellow solid (85% yield). ^{1}H NMR (DMSO-d_6) δ 7.67 (dt, J = 8.6, 2.1 Hz, 1H), 7.54 (d, J = 2.1 Hz, 1H), 7.16 (s, 1H), 7.12 (d, J = 8.6 Hz, 1H), 6.77 (d, J = 7.2 Hz, 1H), 4.66 (br d, J = 9.7 Hz, 1H), 4.16 (q, J = 7.8 Hz, 1H), 4.05 (td, J = 9.3, 5.7 Hz, 1H), 3.88 (s, 3H), 3.84 (s, 3H), 3.78 (s, 3H), 3.74 (s, 3H), 3.54 (m, 1H), 3.51 (m, 1H), 3.21 (m, 1H), 2.09 (m, 2H), 1.86 (m, 2H), 1.58 (m, 2H). ^{13}C NMR (DMSO-d_6) δ 175.5, 167.4, 163.1, 161.4, 160.5, 159.3, 152.2, 149.1, 123.2, 119.6, 111.9, 111.6, 109.1, 107.5, 107.0, 97.1, 80.4, 78.5, 74.2, 71.2, 70.4, 63.3, 62.7, 55.9, 55.7, 43.6, 29.9, 29.9, 14.3. HRESI-TOFMS *m/z* $[M+H]^+$ 572.2120 (calcd for $C_{29}H_{34}NO_{11}^+$, 572.2126, 1.1 ppm error). HPLC purity: 98.3% (210 nm).

(2*S*,3*S*,4*R*,5*R*,6*S*)-*N*-Cyclopentyl-6-(2-(3,4-dimethoxyphenyl)-5,7-dimethoxy-4-oxo-4*H*-chromen-6-yl)-3,4,5-trihydroxytetrahydro-2*H*-pyran-2-carboxamide (16). Light yellow solid (86% yield). ^{1}H NMR (DMSO-d_6) δ 7.66 (d, J = 8.4 Hz, 1H), 7.53 (d, J = 2.1 Hz, 1H), 7.16 (s, 1H), 7.12 (d, J = 8.4 Hz, 1H), 6.75 (d, J = 6.5 Hz, 1H), 4.64 (br d, J = 10.2 Hz, 1H), 3.95 (m,

1H), 3.87 (s, 3H), 3.82 (s, 3H), 3.79 (m, 1H), 3.77 (s, 3H), 3.71 (s, 3H), 3.53 (m, 1H), 3.51 (m, 1H), 3.21 (m, 1H), 1.79 – 1.40 (m, 8H). ^{13}C NMR (DMSO-d_6) δ 175.4, 167.1, 163.6, 161.4, 160.3, 158.8, 152.1, 149.1, 123.0, 119.8, 112.1, 111.8, 109.2, 107.7, 107.1, 97.3, 80.2, 78.5, 74.2, 71.2, 68.6, 63.6, 62.8, 56.3, 55.9, 50.5, 32.1, 32.1, 23.6, 23.6. HRESI-TOFMS *m/z* $[M+H]^+$ 586.2291 (calcd for $C_{30}H_{36}NO_{11}^+$, 586.2283, -1.4 ppm error). HPLC purity: 96.6% (210 nm).

(2*S*,3*S*,4*R*,5*R*,6*S*)-*N*-Cyclohexyl-6-(2-(3,4-dimethoxyphenyl)-5,7-dimethoxy-4-oxo-4*H*-chromen-6-yl)-3,4,5-trihydroxytetrahydro-2*H*-pyran-2-carboxamide (17). Light yellow solid (88% yield). ^{1}H NMR (DMSO-d_6) δ 7.68 (d, J = 8.4 Hz, 1H), 7.55 (d, J = 2.1 Hz, 1H), 7.14 (s, 1H), 7.12 (d, J = 8.4 Hz, 1H), 6.80 (d, J = 6.5 Hz, 1H), 4.65 (br d, J = 10.2 Hz, 1H), 4.04 (q, J = 8.4 Hz, 1H), 3.88 (s, 3H), 3.84 (s, 3H), 3.79 (s, 3H), 3.74 (s, 3H), 3.58 (m, 1H), 3.51 (m, 1H), 3.49 (m, 1H), 3.21 (m, 1H), 1.74 – 1.47 (m, 6H), 1.27 – 0.99 (m, 4H). ^{13}C NMR (DMSO-d_6) δ 175.5, 167.2, 163.2, 161.3, 160.3, 158.8, 152.0, 149.1, 123.1, 119.8, 112.0, 111.4, 109.4, 107.2, 107.0, 96.9, 80.5, 79.1, 74.1, 71.6, 70.6, 63.9, 62.7, 56.4, 56.0, 47.8, 32.6, 32.6, 29.1, 24.6, 24.6. HRESI-TOFMS *m/z* $[M+H]^+$ 600.2446 (calcd for $C_{31}H_{38}NO_{11}^+$, 600.2439, -1.1 ppm error). HPLC purity: 98.6 % (210 nm).

(2*S*,3*S*,4*R*,5*R*,6*S*)-*N*-(Cyclohexylmethyl)-6-(2-(3,4-dimethoxyphenyl)-5,7-dimethoxy-4-oxo-4*H*-chromen-6-yl)-3,4,5-trihydroxytetrahydro-2*H*-pyran-2-carboxamide (18). Light yellow solid (88% yield). ^{1}H NMR (DMSO-d_6) δ 7.66 (d, J = 8.7 Hz, 1H), 7.54 (d, J = 2.0 Hz, 1H), 7.13 (s, 1H), 7.11 (d, J = 8.7 Hz, 1H), 6.76 (d, J = 6.2 Hz, 1H), 4.66 (br d, J = 9.9 Hz, 1H), 4.05 (q, J = 9.9 Hz, 1H), 3.87 (s, 3H), 3.83 (s, 3H), 3.78 (s, 3H), 3.73 (s, 3H), 3.61 (m, 1H), 3.48 (m, 1H), 3.23 (m, 1H), 2.87 (m, 2H), 1.69 – 1.47 (m, 6H), 1.33 (m, 1H), 1.08 (m, 2H), 0.80 (m, 2H). ^{13}C NMR (DMSO-d_6) δ 176.0, 167.0, 163.7, 160.8, 160.6, 158.9, 152.0, 149.3, 123.4, 119.7, 112.0, 111.7, 109.3, 107.2, 107.1, 96.2, 80.3, 78.7, 74.7, 71.3, 69.9, 63.8, 63.1, 56.9, 56.2,

45.1, 37.1, 30.6, 30.6, 26.3, 25.7, 25.7. HRESI-TOFMS *m/z* $[M+H]^+$ 614.2597 (calcd for $C_{32}H_{40}NO_{11}^+$, 614.2596, -0.1 ppm error). HPLC purity: 98.3% (210 nm).

(2*S*,3*S*,4*R*,5*R*,6*S*)-*N*-(Adamantan-1-yl)-6-(2-(3,4-dimethoxyphenyl)-5,7-dimethoxy-4-oxo-4*H*-chromen-6-yl)-3,4,5-trihydroxytetrahydro-2*H*-pyran-2-carboxamide (19). Light yellow solid (81% yield). ^{1}H NMR (DMSO-d_6) δ 7.67 (d, J = 8.4 Hz, 1H), 7.54 (d, J = 2.1 Hz, 1H), 7.13 (s, 1H), 7.12 (d, J = 8.4 Hz, 1H), 6.78 (d, J = 6.8 Hz, 1H), 4.65 (br d, J = 10.2 Hz, 1H), 4.03 (m, 1H), 3.88 (s, 3H), 3.84 (s, 3H), 3.80 (s, 3H), 3.74 (s, 3H), 3.57 (m, 1H), 3.52 (m, 1H), 3.49 (m, 1H), 1.96 (m, 3H), 1.88 – 1.57 (m, 12H). ^{13}C NMR (DMSO-d_6) δ 175.3, 167.2, 163.3, 161.1, 160.2, 158.9, 152.1, 149.2, 123.2, 119.8, 112.1, 111.6, 109.5, 107.2, 107.0, 97.0, 80.7, 79.2, 74.2, 71.7, 70.5, 63.9, 62.5, 56.4, 56.0, 51.2, 41.2, 41.2, 41.2, 36.1, 36.1, 36.1, 28.9, 28.9, 28.9. HRESI-TOFMS *m/z* $[M+H]^+$ 652.2764 (calcd for $C_{35}H_{42}NO_{11}^+$, 652.2752, -1.8 ppm error). HPLC purity: 97.7% (210 nm).

(2*S*,3*S*,4*R*,5*R*,6*S*)-6-(2-(3,4-Dimethoxyphenyl)-5,7-dimethoxy-4-oxo-4*H*-chromen-6-yl)-3,4,5-trihydroxy-*N*-phenyltetrahydro-2*H*-pyran-2-carboxamide (20). Light yellow solid (88% yield). ^{1}H NMR (DMSO-d_6) δ 7.66 (dd, J = 8.6, 2.2 Hz, 1H), 7.62 (dd, J = 8.2, 2.5 Hz, 2H), 7.55 (d, J = 2.2 Hz, 1H), 7.28 (td, J = 8.1, 2.2 Hz, 2H), 7.16–7.10 (m, 2H), 7.03 (t, J = 7.4 Hz, 1H), 6.77 (d, J = 6.5 Hz, 1H), 4.75 (br d, J = 9.7 Hz, 1H), 4.12 (td, J = 9.7, 2.4 Hz, 1H), 3.94 (s, 3H), 3.89 (s, 3H), 3.85 (s, 3H), 3.84 (m, 1H), 3.79 (s, 3H), 3.66 (m, 1H), 3.29 (m, 1H). ^{13}C NMR (DMSO-d_6) δ 175.4, 167.3, 163.4, 161.9, 160.3, 158.8, 151.8, 149.1, 138.8, 128.6, 128.6, 123.4, 123.1, 119.5, 119.3, 119.3, 112.0, 111.8, 109.4, 107.1, 106.9, 97.1, 81.0, 78.6, 73.7, 71.2, 69.6, 63.4, 62.7, 56.5, 56.0. HRESI-TOFMS *m/z* $[M+H]^+$ 594.1986 (calcd for $C_{31}H_{32}NO_{11}^+$, 594.1970, -2.8 ppm error). HPLC purity: 96.5% (210 nm).

(2*S*,3*S*,4*R*,5*R*,6*S*)-6-(2-(3,4-Dimethoxyphenyl)-5,7-dimethoxy-4-oxo-4*H*-chromen-6-yl)-3,4,5-trihydroxy-*N*-benzyltetrahydro-2*H*-pyran-2-carboxamide (21). Light yellow solid (92% yield). ^{1}H NMR (500 MHz, DMSO-d_6) δ 7.67 (d, J = 10.2 Hz, 1H), 7.54 (d, J = 2.1 Hz, 1H), 7.29 – 7.16 (m, 5H), 7.16 – 7.08 (m, 2H), 6.80 (d, J = 6.7 Hz, 1H), 4.68 (dd, J = 9.8, 6.7 Hz, 1H), 4.27 (m, 2H), 4.10 (m, 1H), 3.87 (s, 3H), 3.83 (s, 3H), 3.79 (s, 3H), 3.75 (s, 3H), 3.71 (m, 1H), 3.57 (m, 1H), 3.26 (m, 1H). ^{13}C NMR (DMSO-d_6) δ 175.6, 169.1, 163.6, 162.0, 160.3, 158.9, 151.8, 149.1, 139.2, 128.2, 128.2, 127.3, 127.3, 126.7, 123.1, 119.6, 112.1, 111.7, 109.2, 107.1, 107.0, 97.1, 80.2, 78.8, 73.7, 71.6, 71.0, 63.5, 62.8, 56.6, 56.0, 42.0. HRESI-TOFMS *m/z* $[M+H]^+$ 608.2130 (calcd for $C_{32}H_{34}NO_{11}^+$, 608.2126, -0.5 ppm error). HPLC purity: 97.1% (210 nm).

(2*S*,3*S*,4*R*,5*R*,6*S*)-6-(2-(3,4-Dimethoxyphenyl)-5,7-dimethoxy-4-oxo-4*H*-chromen-6-yl)-3,4,5-trihydroxy-*N*-(pyridin-4-yl)tetrahydro-2*H*-pyran-2-carboxamide (22). Light yellow solid (81% yield). ^{1}H NMR (500 MHz, DMSO-d_6) δ 8.40 (d, J = 5.0 Hz, 2H), 7.68 (d, J = 8.5 Hz, 1H), 7.60 (d, J = 5.0 Hz, 2H), 7.55 (s, 1H), 7.15 (s, 1H), 7.12 (d, J = 8.5 Hz, 1H), 6.81 (d, J = 6.9 Hz, 1H), 4.72 (br d, J = 9.7 Hz, 1H), 4.11 (td, J = 9.2, 4.1 Hz, 1H), 3.94 (m, 1H), 3.88 (s, 3H), 3.84 (s, 3H), 3.83 (s, 3H), 3.76 (s, 3H), 3.62 (m, 1H), 3.29 (m, 1H). ^{13}C NMR (DMSO-d_6) δ 175.6, 167.5, 163.3, 161.7, 160.2, 158.7, 152.0, 150.9, 150.9, 149.2, 145.3, 123.1, 119.9, 112.1, 113.9, 113.9, 111.5, 109.8, 107.5, 106.8, 97.1, 81.2, 78.8, 74.4, 71.5, 69.8, 63.9, 63.0, 56.5, 56.1. HRESI-TOFMS *m/z* $[M+H]^+$ 595.1921 (calcd for $C_{30}H_{31}N_2O_{11}^+$, 595.1922, 0.1 ppm error). HPLC purity: 97.8% (210 nm).

(2*S*,3*S*,4*R*,5*R*,6*S*)-6-(2-(3,4-Dimethoxyphenyl)-5,7-dimethoxy-4-oxo-4*H*-chromen-6-yl)-3,4,5-trihydroxy-*N*-(thiazol-2-yl)tetrahydro-2*H*-pyran-2-carboxamide (23). Light yellow solid (80% yield). ^{1}H NMR (DMSO-d_6) δ 7.68 (d, J = 8.8 Hz, 1H), 7.56 (d, J = 2.0 Hz, 1H), 7.53

(d, J = 1.7 Hz, 1H), 7.18 (d, J = 1.7 Hz, 1H), 7.17 (s, 1H), 7.12 (d, J = 8.8 Hz, 1H), 6.82 (d, J = 6.8 Hz, 1H), 4.67 (br d, J = 10.5 Hz, 1H), 4.03 (m, 1H), 3.89 (s, 3H), 3.84 (s, 3H), 3.82 (s, 3H), 3.76 (s, 3H), 3.60 (m, 1H), 3.55 (m, 1H), 3.23 (m, 1H). ^{13}C NMR (DMSO-d_6) δ 175.4, 168.5, 163.2, 162.3, 161.6, 160.5, 158.9, 151.9, 149.2, 137.2, 123.3, 119.8, 114.1, 111.9, 111.5, 109.5, 107.3, 105.8, 97.3, 80.0, 79.2, 74.3, 72.1, 70.3, 63.7, 62.9, 56.2, 56.0. HRESI-TOFMS *m/z* $[M+H]^+$ 601.1493 (calcd for $C_{28}H_{29}N_2O_{11}S^+$, 601.1487, -1.1 ppm error). HPLC purity: 96.8% (210 nm).

(2*S*,3*S*,4*R*,5*R*,6*S*)-6-(2-(3,4-Dimethoxyphenyl)-5,7-dimethoxy-4-oxo-4*H*-chromen-6-yl)-3,4,5-trihydroxy-*N*-(4-fluorophenyl)tetrahydro-2*H*-pyran-2-carboxamide (24). Light yellow solid (88% yield). ^{1}H NMR (DMSO-d_6) δ 7.70 – 7.61 (m, 3H), 7.54 (d, J = 2.1 Hz, 1H), 7.18 – 7.08 (m, 4H), 6.78 (d, J = 7.1 Hz, 1H), 4.72 (dd, J = 12.0, 9.7 Hz, 1H), 4.11 (q, J = 8.7 Hz, 1H), 3.92 (s, 3H), 3.88 (s, 3H), 3.84 (s, 3H), 3.83 (m, 1H), 3.76 (s, 3H), 3.61 (m, 1H), 3.28 (m, 1H). ^{13}C NMR (DMSO-d_6) δ 175.6, 167.4, 162.8, 160.4, 160.1, 158.6, 156.9, 150.7, 149.2, 136.5, 121.2, 121.2, 123.5, 119.8, 115.5, 115.5, 113.5, 111.8, 109.3, 107.0, 105.7, 97.2, 81.2, 78.5, 74.7, 71.7, 70.4, 63.7, 63.0, 56.1, 55.9. HRESI-TOFMS *m/z* $[M+H]^+$ 612.1892 (calcd for $C_{31}H_{31}FNO_{11}^+$, 612.1876, -2.7 ppm error). HPLC purity: 97.1% (210 nm).

(2*S*,3*S*,4*R*,5*R*,6*S*)-6-(2-(3,4-Dimethoxyphenyl)-5,7-dimethoxy-4-oxo-4*H*-chromen-6-yl)-3,4,5-trihydroxy-*N*-(4-fluorobenzyl)tetrahydro-2*H*-pyran-2-carboxamide (25). Light yellow solid (89% yield). ^{1}H NMR (500 MHz, DMSO-d_6) δ 7.68 (d, J = 8.5 Hz, 1H), 7.55 (d, J = 2.1 Hz, 1H), 7.27 (ddd, J = 8.1, 5.4, 2.2 Hz, 2H), 7.18 – 7.06 (m, 4H), 6.80 (d, J = 6.8 Hz, 1H), 4.67 (t, J = 9.3 Hz, 1H), 4.24 (dd, J = 9.9, 9.0 Hz, 2H), 4.07 (m, 1H), 3.88 (s, 3H), 3.84 (s, 3H), 3.78 (s, 3H), 3.74 (s, 3H), 3.69 (m, 1H), 3.54 (m, 1H), 3.24 (m, 1H). ^{13}C NMR (DMSO-d_6) δ 175.7, 169.1, 163.5, 162.0, 161.2, 160.4, 159.0, 151.9, 149.1, 135.4, 129.3, 129.3, 126.5, 119.7, 115.1,

115.1, 111.8, 111.3, 109.3, 107.1, 105.5, 97.2, 80.2, 78.8, 73.7, 71.9, 71.0, 63.6, 62.9, 56.6, 55.9, 41.3. HRESI-TOFMS *m/z* $[M+H]^+$ 626.2043 (calcd for $C_{32}H_{33}FNO_{11}^+$, 626.2032, -1.7 ppm error). HPLC purity: 97.4% (210 nm).

(2*S*,3*S*,4*R*,5*R*,6*S*)-6-(2-(3,4-Dimethoxyphenyl)-5,7-dimethoxy-4-oxo-4*H*-chromen-6-yl)-3,4,5-trihydroxy-*N*-(2-fluoroethyl)tetrahydro-2*H*-pyran-2-carboxamide (26). Light yellow solid (84% yield). ^{1}H NMR (DMSO-d_6) δ 7.68 (d, *J* = 8.7 Hz, 1H), 7.56 (d, *J* = 2.1 Hz, 1H), 7.17 (s, 1H), 7.12 (d, *J* = 8.7 Hz, 1H), 6.82 (d, *J* = 6.6 Hz, 1H), 4.67 (br d, *J* = 10.5 Hz, 1H), 4.45 (m, 1H), 4.35 (m, 1H), 4.07 (t, *J* = 9.2 Hz, 1H), 3.89 (s, 3H), 3.85 (s, 3H), 3.80 (s, 3H), 3.75 (s, 3H), 3.60 (m, 1H), 3.50 (m, 1H), 3.23 (m, 1H), 3.37 (m, 2H). ^{13}C NMR (DMSO-d_6) δ 175.1, 168.6, 163.5, 161.6, 160.5, 158.9, 151.9, 149.2, 123.6, 119.7, 111.8, 111.4, 109.3, 107.2, 105.5, 97.3, 81.7, 79.9, 79.4, 74.3, 72.3, 70.3, 63.5, 62.9, 56.1, 55.9, 39.1. HRESI-TOFMS *m/z* $[M+H]^+$ 564.1892 (calcd for $C_{27}H_{31}FNO_{11}^+$, 564.1876, -2.9 ppm error). HPLC purity: 97.5% (210 nm).

(2*S*,3*S*,4*R*,5*R*,6*S*)-6-(2-(3,4-Dimethoxyphenyl)-5,7-dimethoxy-4-oxo-4*H*-chromen-6-yl)-3,4,5-trihydroxy-*N*-(2,2,2-trifluoroethyl)tetrahydro-2*H*-pyran-2-carboxamide (27). Light yellow solid (85% yield). ^{1}H NMR (DMSO-d_6) δ 7.68 (dd, *J* = 8.5, 2.0 Hz, 1H), 7.56 (d, *J* = 2.0 Hz, 1H), 7.17 (s, 1H), 7.12 (d, *J* = 8.5 Hz, 1H), 6.81 (d, *J* = 7.7 Hz, 1H), 4.68 (br d, *J* = 9.7 Hz, 1H), 4.07 (q, *J* = 9.1 Hz, 1H), 3.89 (s, 3H), 3.85 (s, 3H), 3.78 (s, 3H), 3.75 (s, 3H), 3.69 (m, 1H), 3.48 (m, 1H), 3.67 (m, 2H), 3.21 (m, 1H). ^{13}C NMR (DMSO-d_6) δ 174.5, 169.5, 163.4, 161.3, 160.4, 158.9, 151.8, 149.1, 125.0, 123.4, 119.7, 112.1, 111.2, 109.4, 107.1, 105.4, 97.2, 80.4, 78.5, 74.8, 71.6, 69.5, 63.6, 62.7, 56.3, 55.9, 41.6. HRESI-TOFMS *m/z* $[M+H]^+$ 600.1700 (calcd for $C_{27}H_{29}F_3NO_{11}^+$, 600.1687, -2.2 ppm error). HPLC purity: 96.8% (210 nm).

(2*S*,3*S*,4*R*,5*R*,6*S*)-6-(2-(3,4-Dimethoxyphenyl)-5,7-dimethoxy-4-oxo-4*H*-chromen-6-yl)-3,4,5-trihydroxy-*N*-(3-fluoropropyl)tetrahydro-2*H*-pyran-2-carboxamide (28). Light yellow solid (86% yield). ^{1}H NMR (DMSO-d_6) δ 7.68 (d, J = 8.7 Hz, 1H), 7.56 (d, J = 2.1 Hz, 1H), 7.17 (s, 1H), 7.12 (d, J = 8.7 Hz, 1H), 6.82 (d, J = 6.4 Hz, 1H), 4.66 (br d, J = 10.6 Hz, 1H), 4.46 (m, 1H), 4.37 (m, 1H), 4.07 (m, 1H), 3.89 (s, 3H), 3.85 (s, 3H), 3.80 (s, 3H), 3.74 (s, 3H), 3.59 (m, 1H), 3.50 (m, 1H), 3.22 (m, 1H), 3.12 (m, 2H), 1.83 – 1.68 (m, 2H). ^{13}C NMR (DMSO-d_6) δ 175.1, 168.5, 163.4, 161.6, 160.6, 158.8, 151.9, 149.3, 123.7, 119.8, 111.9, 111.5, 109.6, 107.3, 105.5, 97.3, 81.9, 80.2, 78.8, 74.2, 71.8, 70.6, 63.6, 62.8, 56.2, 55.8, 34.9, 30.0. HRESI-TOFMS *m/z* $[M+H]^+$ 578.2041 (calcd for $C_{28}H_{33}FNO_{11}^+$, 578.2032, -1.6 ppm error). HPLC purity: 98.3% (210 nm).

(2*S*,3*S*,4*R*,5*R*,6*S*)-6-(2-(3,4-Dimethoxyphenyl)-5,7-dimethoxy-4-oxo-4*H*-chromen-6-yl)-3,4,5-trihydroxy-*N*-(3,3,3-trifluoropropyl)tetrahydro-2*H*-pyran-2-carboxamide (29). Light yellow solid (85% yield). ^{1}H NMR (DMSO-d_6) δ 7.68 (d, J = 8.4 Hz, 1H), 7.55 (d, J = 2.2 Hz, 1H), 7.14 (s, 1H), 7.12 (d, J = 8.4 Hz, 1H), 6.81 (d, J = 5.5 Hz, 1H), 4.68 (br d, J = 10.0 Hz, 1H), 4.07 (m, 1H), 3.89 (s, 3H), 3.85 (s, 3H), 3.80 (s, 3H), 3.74 (s, 3H), 3.61 (m, 1H), 3.49 (m, 1H), 3.28 (m, 2H), 3.21 (m, 1H), 2.40 (m, 2H). ^{13}C NMR (DMSO-d_6) δ 174.6, 169.3, 163.4, 161.1, 160.3, 158.7, 151.8, 149.1, 125.7, 123.1, 119.6, 111.7, 110.9, 109.2, 107.0, 105.2, 97.4, 79.6, 78.3, 73.6, 71.6, 69.5, 63.4, 62.7, 56.0, 55.8, 32.8, 32.1. HRESI-TOFMS *m/z* $[M+H]^+$ 614.1857 (calcd for $C_{28}H_{31}F_3NO_{11}^+$, 614.1844, -2.2 ppm error). HPLC purity: 97.2% (210 nm).

(2*S*,3*S*,4*R*,5*R*,6*S*)-6-(2-(3,4-Dimethoxyphenyl)-5,7-dimethoxy-4-oxo-4*H*-chromen-6-yl)-3,4,5-trihydroxy-*N*-((*S*)-1,1,1-trifluoropropan-2-yl)tetrahydro-2*H*-pyran-2-carboxamide (30). Light yellow solid (82% yield). ^{1}H NMR (500 MHz, DMSO-d_6) δ 7.67 (dd, J = 8.5, 2.1 Hz, 1H), 7.55 (d, J = 2.1 Hz, 1H), 7.15 (br s, 1H), 7.12 (d, J = 8.5 Hz, 1H), 6.78 (d, J = 6.2 Hz, 1H),

4.69 (d, J = 9.6 Hz, 1H), 4.55 (m, 1H), 4.07 (m, 1H), 3.89 (s, 3H), 3.85 (s, 3H), 3.79 (s, 3H), 3.76 (s, 3H), 3.71 (m, 1H), 3.56 (m, 1H), 3.24 (m, 1H), 1.23 (d, J = 6.8 Hz, 3H). ^{13}C NMR (125 MHz, DMSO-d_6) δ 175.5, 168.8, 163.5, 161.7, 160.3, 158.6, 152.1, 149.1, 124.4, 123.1, 119.5, 111.8, 111.3, 109.4, 107.7, 106.9, 96.2, 79.8, 78.3, 73.8, 71.3, 70.3, 62.9, 62.7, 55.9, 55.6, 45.1, 13.3. HRESI-TOFMS *m/z* $[M+H]^+$ 614.1843 (calcd for $C_{28}H_{31}F_3NO_{11}^+$, 614.1844, 0.1 ppm error). HPLC purity: 98.1% (210 nm).

(2*S*,3*S*,4*R*,5*R*,6*S*)-6-(2-(3,4-Dimethoxyphenyl)-5,7-dimethoxy-4-oxo-4*H*-chromen-6-yl)-3,4,5-trihydroxy-*N*-((*R*)-1,1,1-trifluoropropan-2-yl)tetrahydro-2*H*-pyran-2-carboxamide (31). Light yellow solid (86% yield). ^{1}H NMR (500 MHz, DMSO-d_6) δ 7.66 (dd, J = 8.5, 2.0 Hz, 1H), 7.55 (d, J = 2.0 Hz, 1H), 7.14 (br s, 1H), 7.12 (d, J = 8.5 Hz, 1H), 6.77 (d, J = 6.4 Hz, 1H), 4.68 (d, J = 9.8 Hz, 1H), 4.54 (m, 1H), 4.06 (m, 1H), 3.88 (s, 3H), 3.84 (s, 3H), 3.79 (s, 3H), 3.75 (s, 3H), 3.71 (m, 1H), 3.55 (m, 1H), 3.24 (m, 1H), 1.23 (d, J = 6.8 Hz, 3H). ^{13}C NMR (125 MHz, DMSO-d_6) δ 175.3, 168.6, 163.4, 161.5, 160.2, 158.5, 152.1, 149.0, 124.2, 123.0, 119.4, 111.6, 111.1, 109.3, 107.6, 106.8, 96.4, 79.7, 78.5, 73.9, 71.2, 70.4, 63.1, 62.5, 55.7, 55.4, 45.1, 13.3. HRESI-TOFMS *m/z* $[M+H]^+$ 614.1847 (calcd for $C_{28}H_{31}F_3NO_{11}^+$, 614.1844, -0.5 ppm error). HPLC purity: 96.5% (210 nm).

Kinase Luminescent Assay. Kinase inhibition was assessed with the ADP-Glo Kinase Assay. For screening, 5 ng/μL of kinase was assayed in a reaction containing 50 ng/μL substrate, 40 mM Tris, pH 7.5, 20 mM $MgCl_2$, 0.1 mg/mL bovine serum albumin, 50 μM dithiothreitol (DTT), 25 μM ATP, varying concentrations of test samples or 5% DMSO as vehicle. The reaction mixture was incubated for 1 h at room temperature followed by the addition of the ADP-Glo reagents according to the manufacturer's protocol. The kinase inhibitor staurosporine was used at 1 μM as a reference control. Each data point was collected in quadruplicate of two independent

experiments. All new analogues were not promiscuous or pan-assay interference compounds as determined with a detergent-based assay.[23, 31]

To study the GSK-3β kinetics, a reaction solution contained 5 ng/μL kinase, 40 mM Tris, pH 7.5, 20 mM $MgCl_2$, 0.1 mg/mL BSA, 50 μM DTT, and varying concentrations of ATP or substrate GS2 (peptide YRRAAVPPSPSLSRHSSPHQ(pS)EDEEE that is derived from human muscle glycogen synthase) versus test samples. The mixture was incubated for 5, 15, 30, and 60 min at room temperature followed by the addition of the ADP-Glo reagents according to the manufacturer's protocol. The Lineweaver−Burk representation is derived from the double reciprocal plotting of the enzyme kinetic data.

Cell Culture. Human neuroblastoma SH-SY5Y cell line (Sigma-Aldrich, Saint Louis, MO) was cultured in DMEM/F12 (v/v 1:1) media supplemented with 2 mM glutamine, 10% heat-inactivated fetal bovine serum (FBS) and 1% antibiotics including penicillin and streptomycin. After reaching 70-80% confluence, cells were then subcultured on poly-L-lysine plates with 10 μM retinoic acid in a reduced serum media (1% FBS) to promote neuronal maturation and differentiation as described.[35] Cell cultures were incubated at 37 °C in a fully humidified atmosphere containing 5% CO_2.

Whole-Cell Lysate GSK-3β Assay. The assay procedure was followed as described.[23] SH-SY5Y cells were washed with phosphate buffered saline (PBS) and lysed with cell extraction buffer containing 10 mM Tris, pH 7.4, 100 mM NaCl, 1 mM EDTA, 1 mM EGTA, 1 mM NaF, 20 mM $Na_4P_2O_7$, 2 mM Na_3VO_4, 1% Triton X-100, 10% glycerol, 0.1% sodium dodecyl sulfate (SDS), 0.5% sodium deoxycholate, 1 mM phenylmethanesulfonyl fluoride (PMSF) and a protease inhibitor cocktail. Lysate was diluted with kinase buffer (40 mM Tris, pH 7.5, 20 mM

$MgCl_2$, 50 μM DTT, 400 μM ATP) to afford a concentration of 5 μg/μL of total protein, and split into aliquots. Recombinant human GSK-3β was fortified into lysate aliquots to a final concentration of 0.25% (wt/wt) of total protein. A lysate aliquot fortified with heat-inactivated GSK-3β was used as a negative control. The fortified lysate aliquots were incubated with test sample or 5% DMSO vehicle at 37 °C for 2 h followed by ELISA analysis. The GSK-3β inhibitor TDZD-8 was used at 10 μM as a reference control.

Human Tau pS396 ELISA. The quantitative determination of phosphorylated human tau at GSK-3β specific pS396 site was conducted by taking 50 μL diluted cell lysate and using a specific antibody against human tau [pS396] in a sandwich ELISA according to the manufacturer's protocol. Tau phosphorylation was quantified by measuring the absorbance at 450 nm in a microtiter plate reader. The analysis was collected in quadruplicate of two independent experiments.

$A\beta_{42}$ Oligomer Preparation. The toxic oligomers of $A\beta_{42}$ were prepared as described.[23] Briefly, lyophilized $A\beta_{42}$ peptide was dissolved in hexafluoroisopropanol, dried under vacuum, and stored at -20 °C. Immediately prior to use, the peptide residue was reconstituted in DMEM/F12 media to make a stock solution at 0.1 mM and incubated at 4 °C for 24 h to form diffusible oligomers. $A\beta_{42}$ oligomers at a final concentration of 10 μM were assayed for cell viability

Anti-$A\beta_{42}$ Neurotoxicity Assay. SH-SY5Y cells were seeded at a density of 3×10^5 cells/mL in a 96-well plate in DMEM/F12 media containing 10 μM retinoic acid and 1% FBS to suppress cell proliferation. Cells were incubated under regular culture conditions for attachment. After 24 h of plating, the cells were pretreated with different concentrations of test samples or the 0.2%

DMSO as a vehicle control for 1 h and then co-incubated with 10 μM $A\beta_{42}$ for 72 h. After the experimental treatment, the cells were subject to a CellTiter 96 AQueous One Solution Cell Proliferation MTX Assay according to the manufacturer's instruction. Staurosporine at 1 μM was used as a reference control for cytotoxicity, while 10 μM TDZD-8 was used as a reference control for GSK-3β inhibition. Each data point was collected in triplicate of two independent experiments.

PAMPA Studies. A 96-well filter plate with 0.45 μm polyvinylidene fluoride (PVDF) membrane was pre-coated with tri-layer phospholipids. 300 μL of sample solutions (20 μM) in 5% DMSO-PBS at pH 7.4 were added to the donor wells. The accepter plate containing 200 μL 5% DMSO-PBS was then placed on top of the donor plate so that the artificial membrane was in contact with the solution below. The PAMPA system was covered with a lid and incubated for 5 h at room temperature. The concentration of compound in the donor and acceptor wells was quantified by LC-ESI-QTOF-MS. Theophylline and atenolol known for their low permeability were used as negative controls, and desipramine known for its high permeability was used as a positive control. Samples were run in quadruplicate. P_e values and R% were calculated according to the manufacturer's instruction.

Docking Studies. Compounds of interest were docked with AutoDock Vina 1.1.2[38, 40] using the X-ray crystallographic structures of GSK-3β (PDB codes 1PYX[42] and 1H8F[43]). To streamline the docking process, the PDB crystallographic structures were treated without water molecules according to the published GSK-3β docking protocols.[17, 40] Proteins were prepared by adding polar hydrogens and Gasteiger charges using AutoDockTools.[40] Ligands were optimized for their energy and geometry using MMFF94 and AM1 force fields prior to docking as described.[60] All bonds of ligands were treated as rotatable except for the aromatic, alkenyl,

carbonyl bonds and rings. The dimensions of the grid map were 30 × 30 × 30 points with a grid-point spacing of 1 Å. Docking was proceeded with an exhaustiveness value of 500 and a maximum output of 100 structures. Re-docking experiments were conducted using the ligands ANP and HEPES for 1PYX and 1H8F, respectively. ANP showed a binding pose at the ATP site of GSK-3β (PDB code 1PYX) with a RMSD of 0.33 Å as compared to its original crystal structure. HEPES showed a binding pose at the substrate site of GSK-3β (PDB code 1H8F) with a RMSD of 0.62 Å as compared to its original crystal structure. AutoDockTools[40] was used to analyze the docking data of compounds of interest on molecular interactions including hydrogen bonds, hydrophobic contact, π-cation interactions, π-π interactions, and multipolar interactions.

Homology Modeling. The GSK-3α homology model was built with the SWISS-MODEL server.[51] The full sequence of human GSK-3α (UniProt code P49840) was obtained from the Universal Protein Resource. The target sequence was searched against BLAST and HHblits databases for evolutionary related protein structures. A total of 4470 templates were found. For each identified template, the template's quality was predicted from features of the target-template alignment. A template of the GSK-3β structure (PDB code 1PYX) showing the highest quality (sequence identity, 82.97%) in the template ranking was selected for model building. The model was built based on the target-template alignment using ProMod3. Coordinates that are conserved between the target and the template were copied from the template to the model. Insertions and deletions were remodeled using a fragment library. Side chains were then rebuilt. Finally, the geometry and energy minimization of the resulting model was performed using the OpenMM molecular mechanics force field. The model quality assessment was performed based on the global and per-residue model quality using the QMEAN scoring function. A detailed homology modeling method was elaborated in Supporting Information S5.

Statistical Analysis. Data were presented as the mean ± SEM or ± SD. The data were analyzed by one-way ANOVA with Tukey's multiple comparison posthoc test and Student *t* test. The *p* values less than 0.05 were considered statistically significant. Analyses were performed using Excel and GraphPad Prism.

ASSOCIATED CONTENT

Supporting Information. The Supporting Information is available free of charge on the ACS Publications website at DOI: XXX.

Docking method validation, tabulated docking scores, predicted docking poses of selected *C*-glycosylflavones with GSK-3β, summary of molecular interaction distances of compound **30** with GSK3β, GSK-3α homology modeling method, protein sequence alignment of GSK-3α/β isoforms, HPLC analysis data, detail of the kinase selectivity screening, LC-MS method for the PAMPA studies, and structures of the reference compounds (PDF).

AUTHOR INFORMATION

Corresponding Author

*E-mail: qingl@hawaii.edu. Fax: (808) 965-3542.

ORCID

Zhibin Liang: 0000-0002-8855-1696

Qing X. Li: 0000-0003-4589-2869

Author Contributions

Z.L. and Q.X.L conceived the research and performed data interpretation. Z.L. designed and performed experiments and conducted data analysis. Z.L. and Q.X.L wrote the manuscript.

Funding Sources

This work was supported in part by the NIH National Institute on Minority Health and Health Disparities grant 8G12MD007601, and by the USDA National Institute of Food and Agriculture, Hatch project HAW5032-R, managed by the College of Tropical Agriculture and Human Resources, University of Hawaii.

Notes

The authors declare no competing financial interest.

ACKNOWLEDGMENTS

We thank Dr. Philip Williams, Dr. Robert Nichols, and Dr. Jon-Paul Bingham, UH-Manoa, for helpful discussions; Dr. Wei Wen Su, UH-Manoa, for the assistance of bioluminescence measurement; Dr. Yong-Soo Kim and Dr. Jinzeng Yang, UH-Manoa, for the assistance of cell culture; and Wesley Yoshida, UH-Manoa NMR facility, for acquiring the NMR spectra.

ABBREVIATIONS

AD, Alzheimer's disease; Aβ42, β-amyloid fragment peptide 1-42; NFT, neurofibrillary tangle; GSK-3, glycogen synthase kinase-3; ERK2, extracellular signal regulated kinase 2; JNK1, c-Jun N-terminal kinase 1; JNK3, c-Jun N-terminal kinase 3; p38α, p38 mitogen-activated protein kinase 14; p38β, mitogen-activated protein kinase 14B, p38γ, mitogen-activated protein kinase 12; p38δ, p38 mitogen-activated protein kinase 13; CDK1/CyclinA, cyclin-dependent kinase 1 with subunit cyclin A; CDK2/CyclinE, cyclin-dependent kinase 2 with subunit cyclin E; CDK3/CyclinE, cyclin-dependent kinase 3 with subunit cyclin E; CDK5/p25, cyclin-dependent

kinase 5 with subunit p25; CDK5/p35, cyclin-dependent kinase 5 with subunit p35; CDK6/CyclinD, cyclin-dependent kinase 6 with subunit cyclin D; CDK9/CyclinK, cyclin-dependent kinase 9 with subunit cyclin K; CLK1, dual specificity protein kinase 1; AKT1, v-akt murine thymoma viral oncogene homolog 1; p70S6Kβ, p70 ribosomal protein S6 kinase beta; PDK1, phosphoinositide-dependent kinase 1; PKA, protein kinase A; PKC, protein kinase C; PRKG1, cGMP-dependent protein kinase 1; ROCK1, Rho-associated, coiled-coil containing protein kinase 1; RSK2, ribosomal protein S6 kinase 2; AMPK, AMP-activated protein kinase with subunits; CAMKIIα, Ca2+/calmodulin-dependent protein kinase IIα; CAMKIIγ, Ca2+/calmodulin-dependent protein kinase IIγ; CAMKIV, Ca2+/calmodulin-dependent protein kinase IV; DAPK1, death-associated protein kinase 1; STK33, serine/threonine-protein kinase 33; CK2α1, casein kinase 2α1; DNA-PK, DNA-dependent protein kinase; CK1α1, casein kinase 1α1; CK1ε, casein kinase 1ε; CK1γ1, casein kinase 1γ1; VRK2, vaccinia related kinase 2; ANP, adenylyl imidodiphosphate; HEPES, 4-(2-hydroxyethyl)piperazine-1-ethanesulfonic acid; $TMSCHN_2$, trimethylsilyldiazomethane; HCTU, 2-(6-chloro-1-*H*-benzotriazole-1-yl)-1,1,3,3-tetramethylaminium hexafluorophosphate; DIPEA, *N*,*N*-diisopropylethylamine; $[TEMPO]^+[BF_4]^-$, 4-acetamido-2,2,6,6-tetramethyl-1-oxopiperidinium tetrafluoroborate; TDZDs, thiadiazolidinones; CLog*P*, calculated logarithm of partition coefficient; LiPE, ligand-lipophilic efficiency; SAR, structure-activity relationship; ELISA, enzyme-linked immunosorbent assay; PAMPA, parallel artificial membrane permeability assay; HPLC, high performance liquid chromatography; LC-ESI-QTOF-MS, liquid chromatography-electrospray ionization-quadrupole time-of-flight-mass spectrometry; HRMS, high resolution mass spectrometry; NMR, nuclear magnetic resonance.

REFERENCES

(1) Querfurth, H. W., and LaFerla, F. M. (2010) Alzheimer's disease, *N. Engl. J. Med. 362*, 329-344.

(2) McDade, E., and Bateman, R. J. (2017) Stop Alzheimer's before it starts, *Nature 547*, 153-155.

(3) Hoover, B. R., Reed, M. N., Su, J., Penrod, R. D., Kotilinek, L. A., Grant, M. K., Pitstick, R., Carlson, G. A., Lanier, L. M., Yuan, L.-L., Ashe, K. H., and Liao, D. (2010) Tau mislocalization to dendritic spines mediates synaptic dysfunction independently of neurodegeneration, *Neuron 68*, 1067-1081.

(4) Khanna, M. R., Kovalevich, J., Lee, V. M. Y., Trojanowski, J. Q., and Brunden, K. R. (2016) Therapeutic strategies for the treatment of tauopathies: Hopes and challenges, *Alzheimers Dement. 12*, 1051-1065.

(5) Reardon, S. (2015) Alzheimer antibody drugs show questionable potential, *Nat. Rev. Drug Discov. 14*, 591-592.

(6) Honig, L. S., Vellas, B., Woodward, M., Boada, M., Bullock, R., Borrie, M., Hager, K., Andreasen, N., Scarpini, E., Liu-Seifert, H., Case, M., Dean, R. A., Hake, A., Sundell, K., Hoffmann, V. P., Carlson, C., Khanna, R., Mintun, M., DeMattos, R., Selzler, K. J., and Siemers, E. (2018) Trial of solanezumab for mild dementia due to Alzheimer's disease, *N. Engl. J. Med. 378*, 321-330.

(7) Iqbal, K., Liu, F., and Gong, C.-X. (2016) Tau and neurodegenerative disease: The story so far, *Nat. Rev. Neurol. 12*, 15-27.

(8) Hooper, C., Killick, R., and Lovestone, S. (2008) The GSK3 hypothesis of Alzheimer's disease, *J. Neurochem. 104*, 1433-1439.

(9) Martin, L., Latypova, X., Wilson, C. M., Magnaudeix, A., Perrin, M.-L., Yardin, C., and Terro, F. (2013) Tau protein kinases: Involvement in Alzheimer's disease, *Ageing Res. Rev. 12*, 289-309.

(10) Schneider, L. S., Mangialasche, F., Andreasen, N., Feldman, H., Giacobini, E., Jones, R., Mantua, V., Mecocci, P., Pani, L., Winblad, B., and Kivipelto, M. (2014) Clinical trials and late-stage drug development for Alzheimer's disease: An appraisal from 1984 to 2014, *J. Intern. Med. 275*, 251-283.

(11) Pandey, M. K., and DeGrado, T. R. (2016) Glycogen synthase kinase-3 (GSK-3) – targeted therapy and imaging, *Theranostics 6*, 571-593.

(12) Domínguez, J. M., Fuertes, A., Orozco, L., del Monte-Millán, M., Delgado, E., and Medina, M. (2012) Evidence for irreversible inhibition of glycogen synthase kinase-3β by tideglusib, *J. Biol. Chem. 287*, 893-904.

(13) Swinney, Z. T., Haubrich, B. A., Xia, S., Ramesha, C., Gomez, S. R., Guyett, P., Mensa-Wilmot, K., and Swinney, D. C. (2016) A four-point screening method for assessing molecular mechanism of action (MMOA) identifies tideglusib as a time-dependent inhibitor of Trypanosoma brucei GSK3β, *PLoS Negl. Trop. Dis. 10*, e0004506.

(14) Huggins, D. J., Sherman, W., and Tidor, B. (2012) Rational approaches to improving selectivity in drug design, *J. Med. Chem. 55*, 1424-1444.

(15) Peng, J., Kudrimoti, S., Prasanna, S., Odde, S., Doerksen, R. J., Pennaka, H. K., Choo, Y.-M., Rao, K. V., Tekwani, B. L., Madgula, V., Khan, S. I., Wang, B., Mayer, A. M. S., Jacob, M. R., Tu, L. C., Gertsch, J., and Hamann, M. T. (2010) Structure-activity relationship and mechanism of action studies of manzamine analogues for the control of neuroinflammation and cerebral infections, *J. Med. Chem. 53*, 61-76.

(16) Palomo, V., Perez, D. I., Perez, C., Morales-Garcia, J. A., Soteras, I., Alonso-Gil, S., Encinas, A., Castro, A., Campillo, N. E., Perez-Castillo, A., Gil, C., and Martinez, A. (2012) 5-Imino-1,2,4-thiadiazoles: First small molecules as substrate competitive inhibitors of glycogen synthase kinase 3, *J. Med. Chem. 55*, 1645-1661.

(17) Tapia-Rojas, C., Schüller, A., Lindsay, C. B., Ureta, R. C., Mejías-Reyes, C., Hancke, J., Melo, F., and Inestrosa, N. C. (2015) Andrographolide activates the canonical Wnt signalling pathway by a mechanism that implicates the non-ATP competitive inhibition of GSK-3β: Autoregulation of GSK-3β in vivo., *Biochem. J. 466*, 415-430.

(18) Licht-Murava, A., Paz, R., Vaks, L., Avrahami, L., Plotkin, B., Eisenstein, M., and Eldar-Finkelman, H. (2016) A unique type of GSK-3 inhibitor brings new opportunities to the clinic, *Sci. Signal. 9*, ra110.

(19) Rodrigues, T., Reker, D., Schneider, P., and Schneider, G. (2016) Counting on natural products for drug design, *Nature Chem. 8*, 531-541.

(20) Baptista, F. I., Henriques, A. G., Silva, A. M. S., Wiltfang, J., and da Cruz e Silva, O. A. B. (2014) Flavonoids as therapeutic compounds targeting key proteins involved in Alzheimer's disease, *ACS Chem. Neurosci. 5*, 83-92.

(21) Xiao, J., Capanoglu, E., Jassbi, A. R., and Miron, A. (2016) Advance on the flavonoid C-glycosides and health benefits, *Crit. Rev. Food Sci. Nutr. 56*, S29-S45.

(22) Sciacca, M. F. M., Romanucci, V., Zarrelli, A., Monaco, I., Lolicato, F., Spinella, N., Galati, C., Grasso, G., D'Urso, L., Romeo, M., Diomede, L., Salmona, M., Bongiorno, C., Di Fabio, G., La Rosa, C., and Milardi, D. (2017) Inhibition of Aβ amyloid growth and toxicity by silybins: The crucial role of stereochemistry, *ACS Chem. Neurosci. 8*, 1767-1778.

(23) Liang, Z., Zhang, B., Su, W. W., Williams, P. G., and Li, Q. X. (2016) C-Glycosylflavones alleviate tau phosphorylation and amyloid neurotoxicity through GSK3β inhibition, *ACS Chem. Neurosci. 7*, 912-923.

(24) Song, Y., Kim, H.-D., Lee, M.-K., Hong, I.-H., Won, C.-K., Bai, H.-W., Lee, S. S., Lee, S., Chung, B. Y., and Cho, J.-H. (2017) Maysin and its flavonoid derivative from centipedegrass attenuates amyloid plaques by inducting humoral immune response with Th2 skewed cytokine response in the Tg (APPswe, PS1dE9) Alzheimer's mouse model, *PLoS ONE 12*, e0169509.

(25) Peng, K.-Z., Zhang, S.-Y., and Zhou, H.-L. (2016) Toxicological evaluation of the flavonoid-rich extract from Maydis stigma: Subchronic toxicity and genotoxicity studies in mice, *J. Ethnopharmacol. 192*, 161-169.

(26) Ilouz, R., Kowalsman, N., Eisenstein, M., and Eldar-Finkelman, H. (2006) Identification of novel glycogen synthase kinase-3β substrate-interacting residues suggests a common mechanism for substrate recognition, *J. Biol. Chem. 281*, 30621-30630.

(27) Walle, T. (2007) Methylation of dietary flavones greatly improves their hepatic metabolic stability and intestinal absorption, *Mol. Pharm. 4*, 826-832.

(28) Liang, Z., Sorribas, A., Sulzmaier, F. J., Jiménez, J. I., Wang, X., Sauvage, T., Yoshida, W. Y., Wang, G., Ramos, J. W., and Williams, P. G. (2011) Stictamides A–C, MMP12 inhibitors containing 4-amino-3-hydroxy-5-phenylpentanoic acid subunits, *J. Org. Chem. 76*, 3635-3643.

(29) Bobbitt, J. M., Bartelson, A. L., Bailey, W. F., Hamlin, T. A., and Kelly, C. B. (2014) Oxoammonium salt oxidations of alcohols in the presence of pyridine bases, *J. Org. Chem. 79*, 1055-1067.

(30) Baell, J. B. (2016) Feeling nature's PAINS: Natural products, natural product drugs, and pan assay interference compounds (PAINS), *J. Nat. Prod. 79*, 616-628.

(31) Feng, B. Y., and Shoichet, B. K. (2006) A detergent-based assay for the detection of promiscuous inhibitors, *Nat. Protoc. 1*, 550-553.

(32) Wager, T. T., Hou, X., Verhoest, P. R., and Villalobos, A. (2016) Central nervous system multiparameter optimization desirability: Application in drug discovery, *ACS Chem. Neurosci. 7*, 767-775.

(33) Freeman-Cook, K. D., Hoffman, R. L., and Johnson, T. W. (2013) Lipophilic efficiency: The most important efficiency metric in medicinal chemistry, *Future Med. Chem. 5*, 113-115.

(34) Chou, J. T., and Jurs, P. C. (1979) Computer-assisted computation of partition coefficients from molecular structures using fragment constants, *J. Chem. Inf. Comput. Sci. 19*, 172-178.

(35) Agholme, L., Lindström, T., Kågedal, K., Marcusson, J., and Hallbeck, M. (2010) An in vitro model for neuroscience: Differentiation of SH-SY5Y cells into cells with morphological and biochemical characteristics of mature neurons, *J. Alzheimer's Dis. 20*, 1069-1082.

(36) Chen, X., Murawski, A., Patel, K., Crespi, C. L., and Balimane, P. V. (2008) A novel design of artificial membrane for improving the PAMPA model, *Pharm. Res. 25*, 1511-1520.

(37) Courts, F. L., and Williamson, G. (2015) The occurrence, fate and biological activities of C-glycosyl flavonoids in the human diet, *Crit. Rev. Food Sci. Nutr. 55*, 1352-1367.

(38) Trott, O., and Olson, A. J. (2010) AutoDock Vina: Improving the speed and accuracy of docking with a new scoring function, efficient optimization, and multithreading, *J. Comput. Chem. 31*, 455-461.

(39) Wang, Z., Sun, H., Yao, X., Li, D., Xu, L., Li, Y., Tian, S., and Hou, T. (2016) Comprehensive evaluation of ten docking programs on a diverse set of protein-ligand

complexes: The prediction accuracy of sampling power and scoring power, *Phys. Chem. Chem. Phys. 18*, 12964-12975.

(40) Forli, S., Huey, R., Pique, M. E., Sanner, M. F., Goodsell, D. S., and Olson, A. J. (2016) Computational protein-ligand docking and virtual drug screening with the AutoDock suite, *Nat. Protoc. 11*, 905-919.

(41) Hassandarvish, P., Rothan, H. A., Rezaei, S., Yusof, R., Abubakar, S., and Zandi, K. (2016) In silico study on baicalein and baicalin as inhibitors of dengue virus replication, *RSC Advances 6*, 31235-31247.

(42) Bertrand, J. A., Thieffine, S., Vulpetti, A., Cristiani, C., Valsasina, B., Knapp, S., Kalisz, H. M., and Flocco, M. (2003) Structural characterization of the GSK-3β active site using selective and non-selective ATP-mimetic inhibitors, *J. Mol. Biol. 333*, 393-407.

(43) Dajani, R., Fraser, E., Roe, S. M., Young, N., Good, V., Dale, T. C., and Pearl, L. H. (2001) Crystal structure of glycogen synthase kinase 3β: Structural basis for phosphate-primed substrate specificity and autoinhibition, *Cell 105*, 721-732.

(44) Gadakar, P. K., Phukan, S., and Balaji, V. N. (2007) Pose prediction accuracy in docking studies and enrichment of actives in the active site of GSK-3β, *J. Chem. Inf. Model. 47*, 1446-1459.

(45) Fu, G., Sivaprakasam, P., Dale, O. R., Manly, S. P., Cutler, S. J., and Doerksen, R. J. (2014) Pharmacophore modeling, ensemble docking, virtual screening, and biological evaluation on glycogen synthase kinase-3β, *Mol. Inform. 33*, 610-626.

(46) Müller, K., Faeh, C., and Diederich, F. (2007) Fluorine in pharmaceuticals: Looking beyond intuition, *Science 317*, 1881-1886.

(47) Bissantz, C., Kuhn, B., and Stahl, M. (2010) A medicinal chemist's guide to molecular interactions, *J. Med. Chem. 53*, 5061-5084.

(48) Abreu, R. M. V., Froufe, H. J. C., Queiroz, M.-J. R. P., and Ferreira, I. C. F. R. (2012) Selective flexibility of side-chain residues improves VEGFR-2 docking score using AutoDock Vina, *Chem. Biol. Drug Des. 79*, 530-534.

(49) Gallivan, J. P., and Dougherty, D. A. (1999) Cation-π interactions in structural biology, *Proc. Natl. Acad. Sci. U.S.A. 96*, 9459-9464.

(50) Pellequer, J.-L., Zhao, B., Kao, H.-I., Bell, C. W., Li, K., Li, Q. X., Karu, A. E., and Roberts, V. A. (2000) Stabilization of bound polycyclic aromatic hydrocarbons by a π-cation interaction, *J. Mol. Biol. 302*, 691-699.

(51) Biasini, M., Bienert, S., Waterhouse, A., Arnold, K., Studer, G., Schmidt, T., Kiefer, F., Cassarino, T. G., Bertoni, M., Bordoli, L., and Schwede, T. (2014) SWISS-MODEL: Modelling protein tertiary and quaternary structure using evolutionary information, *Nucleic Acids Res. 42*, W252-W258.

(52) Beurel, E., Grieco, S. F., and Jope, R. S. (2015) Glycogen synthase kinase-3 (GSK3): Regulation, actions, and diseases, *Pharmacol. Ther. 148*, 114-131.

(53) Liang, S. H., Chen, J. M., Normandin, M. D., Chang, J. S., Chang, G. C., Taylor, C. K., Trapa, P., Plummer, M. S., Para, K. S., Conn, E. L., Lopresti-Morrow, L., Lanyon, L. F., Cook, J. M., Richter, K. E. G., Nolan, C. E., Schachter, J. B., Janat, F., Che, Y., Shanmugasundaram, V., Lefker, B. A., Enerson, B. E., Livni, E., Wang, L., Guehl, N. J., Patnaik, D., Wagner, F. F., Perlis, R., Holson, E. B., Haggarty, S. J., El Fakhri, G., Kurumbail, R. G., and Vasdev, N. (2016) Discovery of a highly selective glycogen synthase kinase-3 inhibitor (PF-04802367) that modulates tau phosphorylation in the brain: Translation for PET neuroimaging, *Angew. Chem., Int. Ed. 55*, 9601-9605.

(54) Koehler, M. F. T., Bergeron, P., Blackwood, E. M., Bowman, K., Clark, K. R., Firestein, R., Kiefer, J. R., Maskos, K., McCleland, M. L., Orren, L., Salphati, L., Schmidt, S., Schneider, E. V., Wu, J., and Beresini, M. H. (2016) Development of a potent, specific CDK8 kinase inhibitor which phenocopies CDK8/19 knockout cells, *ACS Med. Chem. Lett. 7*, 223-228.

(55) Wei, J., Jin, F., Wu, Q., Jiang, Y., Gao, D., and Liu, H. (2014) Molecular interaction study of flavonoid derivative 3d with human serum albumin using multispectroscopic and molecular modeling approach, *Talanta 126*, 116-121.

(56) Pollock, J., Borkin, D., Lund, G., Purohit, T., Dyguda-Kazimierowicz, E., Grembecka, J., and Cierpicki, T. (2015) Rational design of orthogonal multipolar interactions with fluorine in protein–ligand complexes, *J. Med. Chem. 58*, 7465-7474.

(57) Ali, A., Hoeflich, K. P., and Woodgett, J. R. (2001) Glycogen synthase kinase-3: Properties, functions, and regulation, *Chem. Rev. 101*, 2527-2540.

(58) Wang, Q. M., Park, I. K., Fiol, C. J., Roach, P. J., and DePaoli-Roach, A. A. (1994) Isoform differences in substrate recognition by glycogen synthase kinases 3.alpha. and 3.beta. in the phosphorylation of phosphatase inhibitor 2, *Biochemistry 33*, 143-147.

(59) Soutar, M. P. M., Kim, W.-Y., Williamson, R., Peggie, M., Hastie, C. J., McLauchlan, H., Snider, W. D., Gordon-Weeks, P. R., and Sutherland, C. (2010) Evidence that glycogen synthase kinase-3 isoforms have distinct substrate preference in the brain, *J. Neurochem. 115*, 974-983.

(60) Liang, Z., Sulzmaier, F. J., Yoshida, W. Y., Kelly, M., Ramos, J. W., and Williams, P. G. (2015) Neopetrocyclamines A and B, polycyclic diamine alkaloids from the sponge Neopetrosia cf exigua, *J. Nat. Prod. 78*, 543-547.

Scheme 1. Chemical Modifications Beginning with Isoorientin [a]

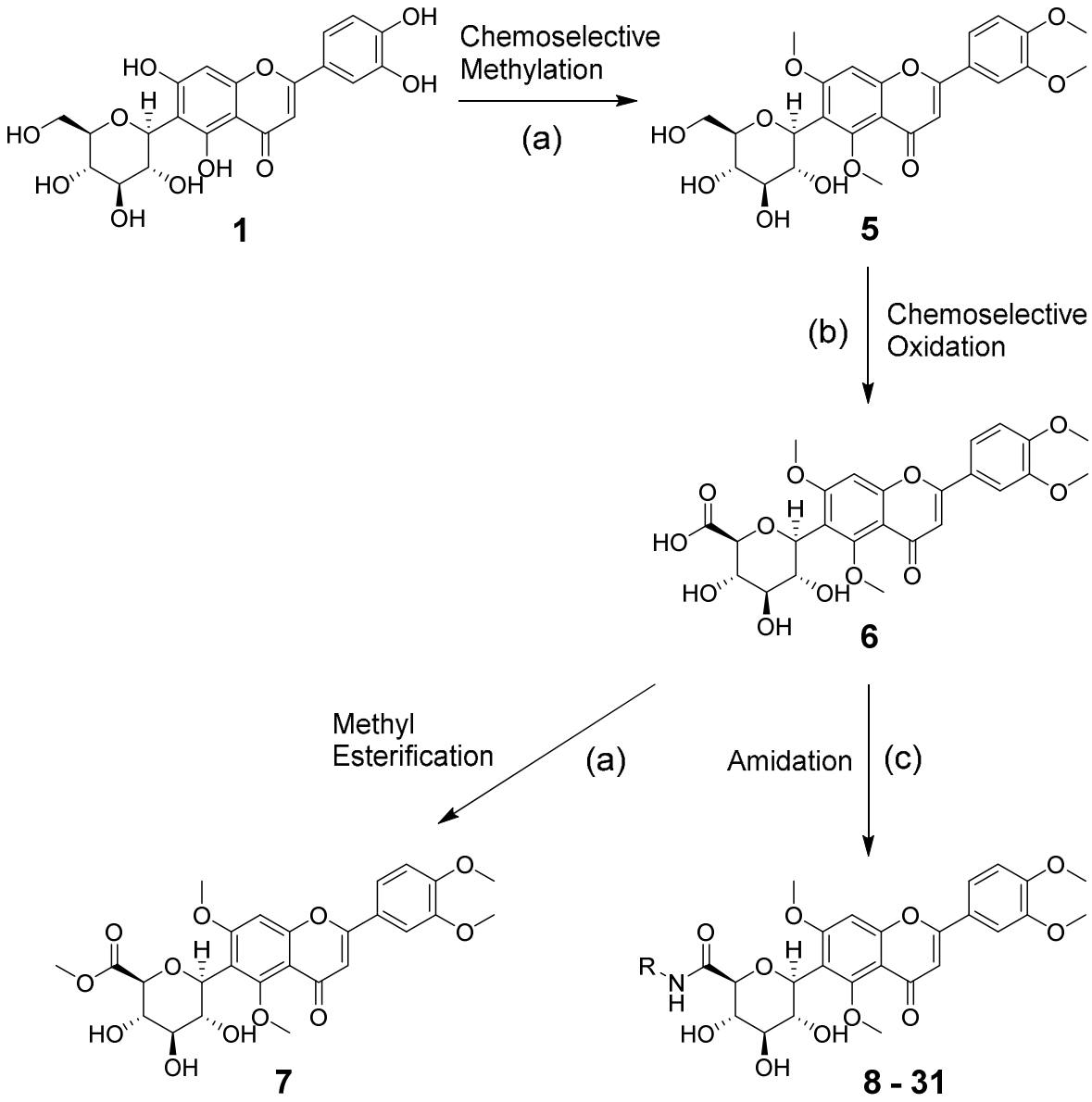

[a] Reagents and conditions: (a) $TMSCHN_2$, toluene, methanol, rt, 80%; (b) $[TEMPO]^+[BF_4]^-$, DCM, pyridine, rt, 95%; (c) R-NH_2, HCTU, DIPEA, DMF, DCM, rt, 80-90%.

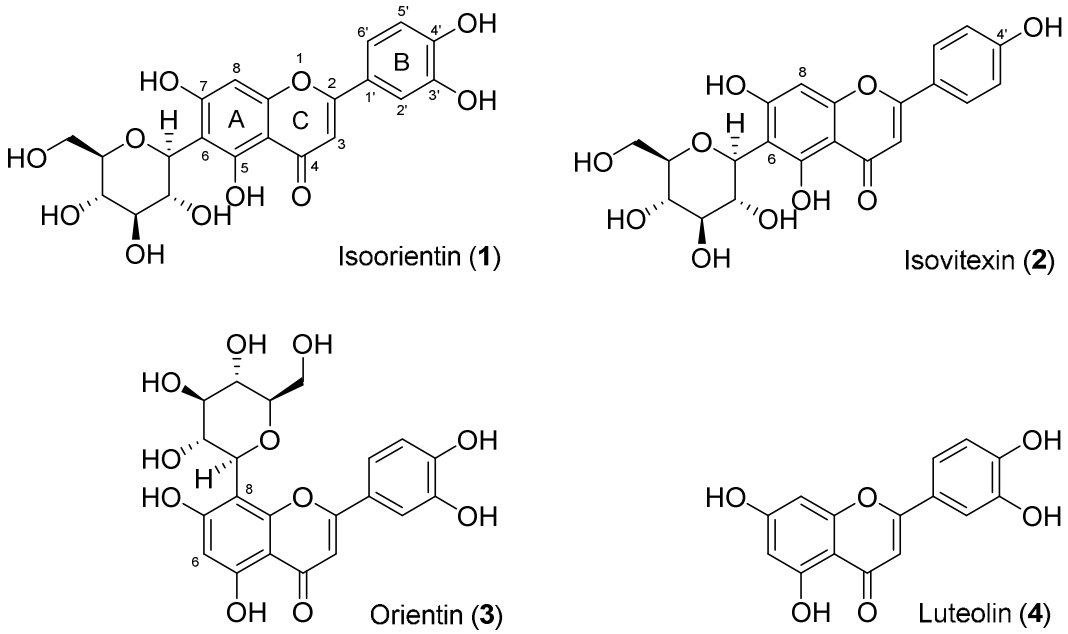

Figure 1. Natural *C*-glycosyl and aglycosyl flavones **1**-**4**.

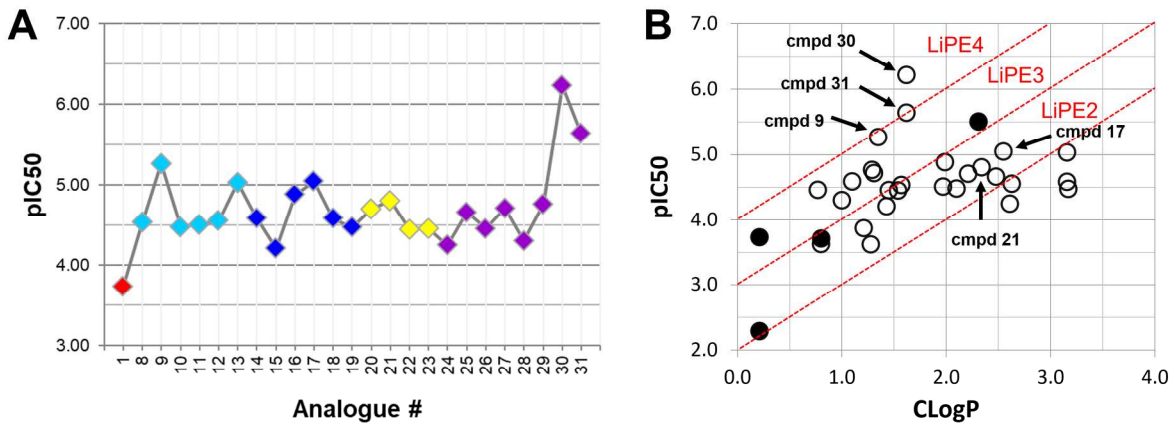

Figure 2. Analyses of GSK-3β inhibitory activities for compounds **1**-**31**. (A) A scatter plot of pIC50 (-LogIC50) for GSK-3β inhibitors **1**, **8**-**31**. The parent compound isoorientin **1** is shown in red, aliphatic amide analogues are shown in cyan, alicyclic amide analogues are shown in blue, aromatic amide analogues are shown in yellow, and fluorinated amide analogues are shown in purple. (B) A plot of CLog*P* versus pIC50 for GSK-3β inhibitors **1**-**31**. Diagonal lines represent areas of the same LiPEs to estimate druglikeness. LiPE = pIC50 – CLog*P*. Solid circle: natural flavones; Open circle: semi-synthetic flavones. cmpd, compound.

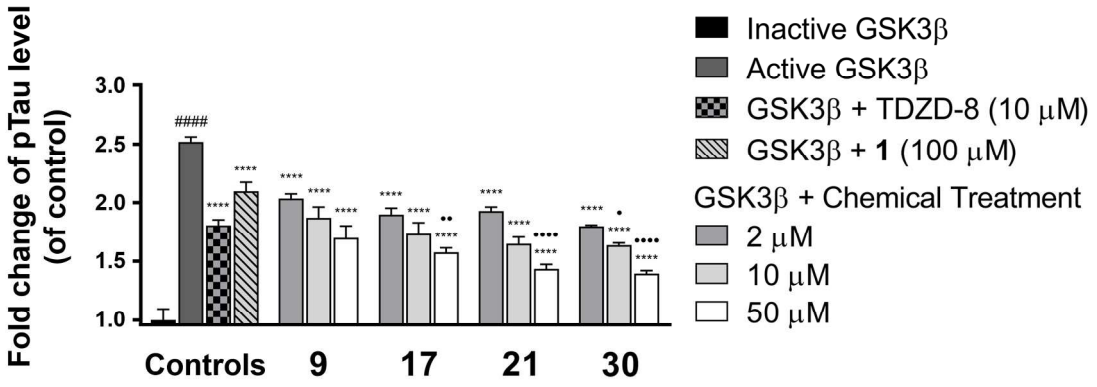

Figure 3. Compounds **9**, **17**, **21** and **30** attenuate GSK-3β-mediated tau phosphorylation in a SH-SY5Y whole-cell lysate kinase assay. Cell lysate aliquots were fortified with 0.25% (wt/wt) GSK-3β, and incubated with 2 to 50 μM of **9**, **17**, **21**, **30** or 5% DMSO vehicle in a kinase buffer at 37 °C for 2 h. 10 μM TDZD-8 and 100 μM isoorientin (**1**) were used as reference controls. ELISA analysis was performed with specific antibody against Tau pS396 to quantify tau phosphorylation levels. Fold changes were calculated relative to the control with ± SEM ($n = 4$). The data were analyzed by one-way ANOVA with Tukey's multiple comparison test. ####$p <$ 0.0001 relative to inactive GSK-3β fortified control; ****$p < 0.0001$ relative to the active GSK-3β fortified control; •$p < 0.05$, ••$p < 0.01$ and ••••$p < 0.0001$ relative to the TDZD-8 reference control.

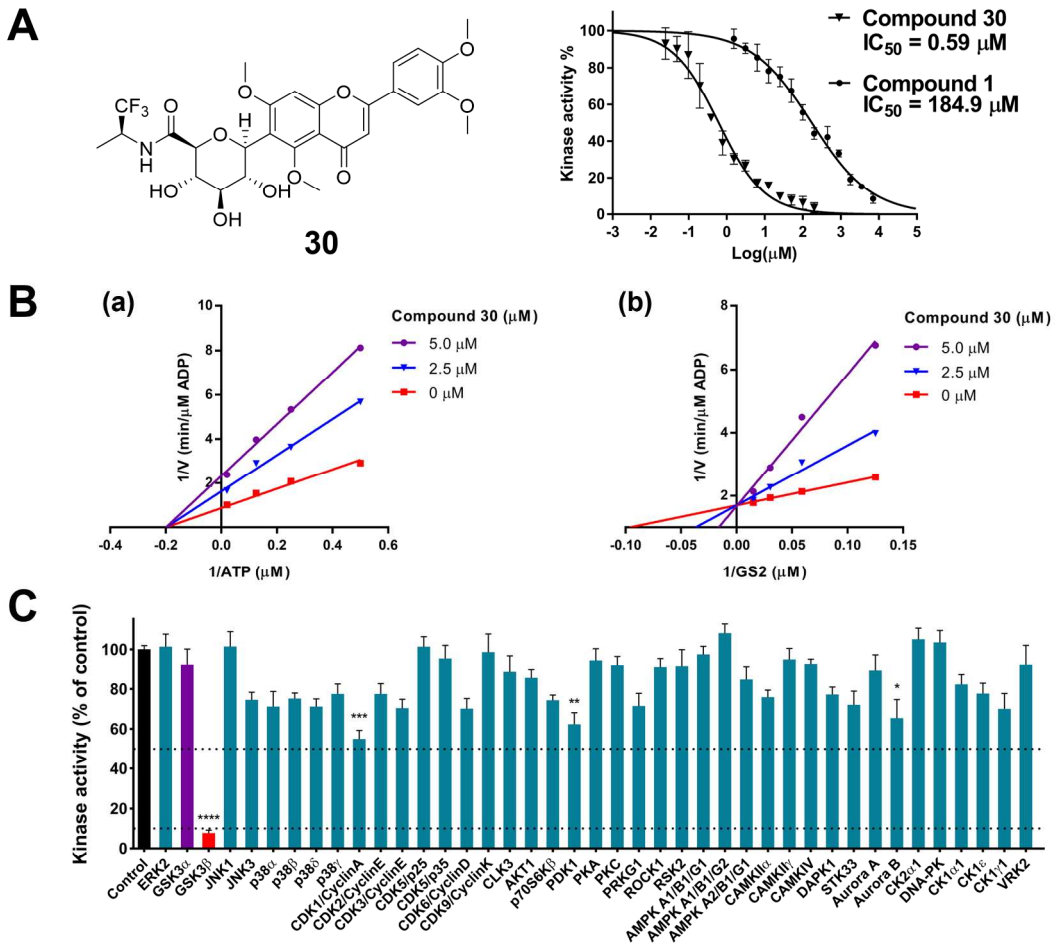

Figure 4. Compound **30** selectively inhibits GSK-3β via a substrate-competitive mechanism. (A) Structure of **30** and inhibition curves of **30** with an IC_{50} of 0.59 μM and **1** with an IC_{50} of 184.9 μM. The results were presented as the percentage of the kinase activity relative to control (5% DMSO vehicle). Inhibition curves were analyzed by four-parameter regression. (B) Lineweaver–Burk plots of GSK-3β kinetic data at increasing concentrations of **30** from 0 to 5 μM. (a) The lines are linear regression plotting of 1/V against 1/ATP at a given concentration of **30**. ATP concentrations varied from 2 to 50 μM, while the concentration of the GSK-3β substrate GS2 was kept constant at 17 μM. Intersecting at the same point on the x-axis indicates noncompetitive inhibition with respect to ATP. (b) The lines are linear regression plotting of 1/V against 1/GS2 at a given concentration of **30**. Substrate GS2 concentrations varied from 8 to 66 μM, while the ATP concentration was kept constant at 10 μM. Intersecting at the same point on the y-axis indicates competitive inhibition with respect to the substrate GS2. (C) Inhibitory effects of **30** on the activities of 41 kinases. Kinases were assayed in the presence of 5 μM **30** or control (5% DMSO vehicle). Data were the mean of quadruplicate of each of two independent experiments with ± SEM. The data were analyzed by one-way ANOVA with Tukey's multiple comparison test. *$p < 0.05$, **$p < 0.01$, ***$p < 0.001$, ****$p < 0.0001$ relative to the control.

1142

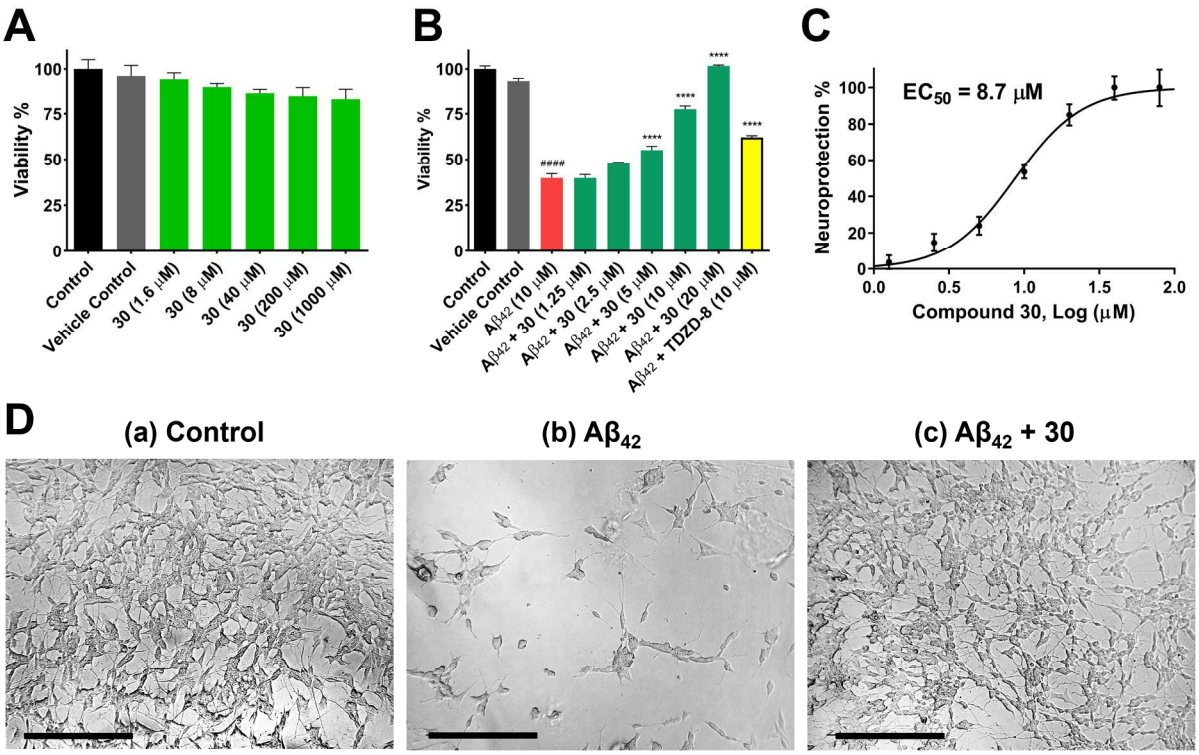

Figure 5. Compound **30** alleviates $A\beta_{42}$ induced neurotoxicity in SH-SY5Y cells. (A) Cytotoxicity assessment of **30** in SH-SY5Y cells. Cells were treated with varying concentrations of **30** or 0.2% DMSO vehicle and incubated for 72 h. Cell viability was determined with the MTX assay. (B) Cells were pretreated with varying concentrations of **30** or 0.2% DMSO vehicle for 1 h followed by 10 μM $A\beta_{42}$ treatment and incubated for 72 h. 10 μM TDZD-8 was used as a reference control. (C) **30** inhibited neurotoxicity induced by 10 μM $A\beta_{42}$ with an EC_{50} value of 8.7 μM. The results were presented as the percentage of the neuroprotective activity relative to control (100%) and 10 μM $A\beta_{42}$ treatment (0%). Neuroprotection curve was analyzed by four-parameter regression. Data were the mean of triplicate of each of two independent experiments with ± SEM. The data were analyzed by one-way ANOVA with Tukey's multiple comparison test. ####$p < 0.0001$ relative to vehicle control; ****$p < 0.0001$ relative to the 10 μM $A\beta_{42}$ treatment. (D) Morphological changes of SH-SY5Y cells after treatment for 72 h. (a) 0.2% DMSO treatment as vehicle control. Differentiated cells with extended axons and dendrites. (b) 10 μM $A\beta_{42}$ treatment. Dying and impaired cells with retracted neurites. (c) Pretreatment of 10 μM **30** followed by 10 μM $A\beta_{42}$ treatment. Protected differentiated cells with extended axons and dendrites. Micrographs represent the average morphologic characteristics of cell cultures under a given condition of 4-6 experimental replicates. Scale bar = 100 μm.

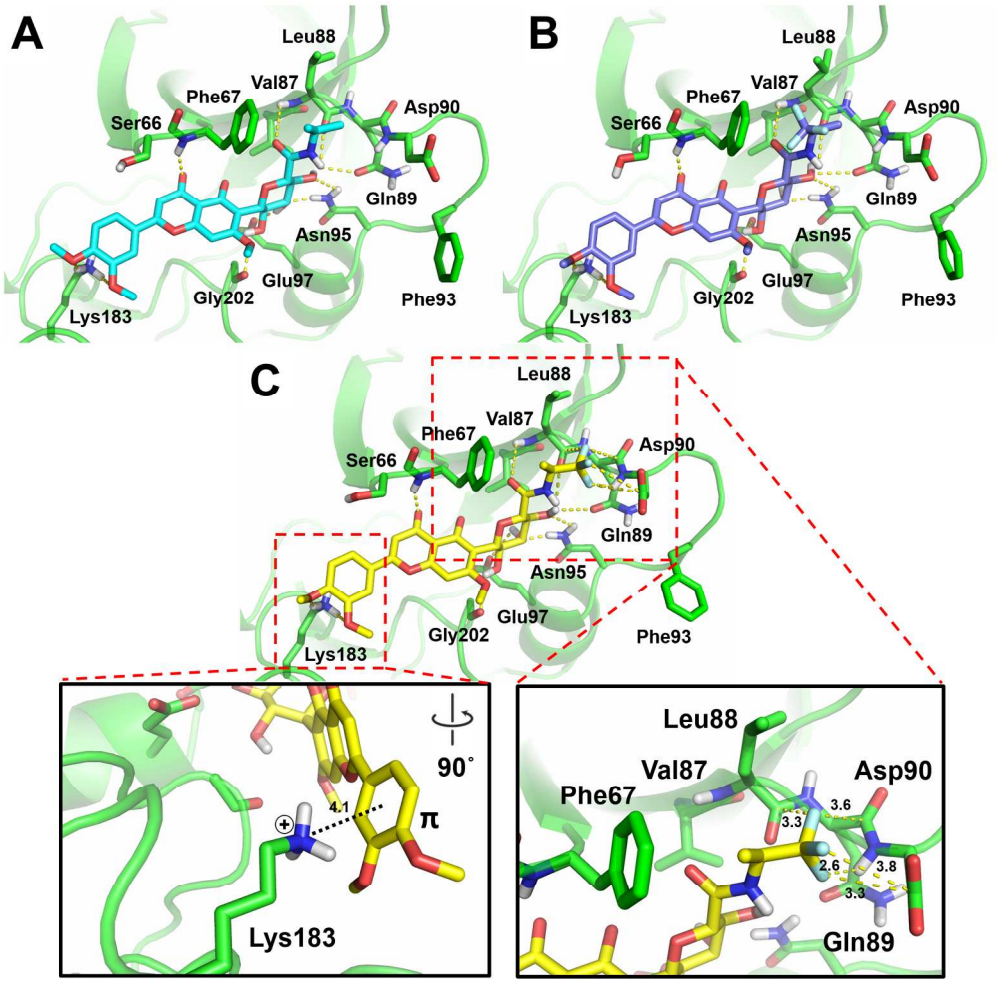

Figure 6. Predicted docking poses of **9** (A), **31** (B) and **30** (C) within the substrate site of GSK-3β (PDB code 1PYX). The dotted lines represent interactions via hydrogen bonding, π-cation interaction or orthogonal multipolar interactions with key amino acid residues of GSK-3β. Key molecular interaction distances are highlighted.

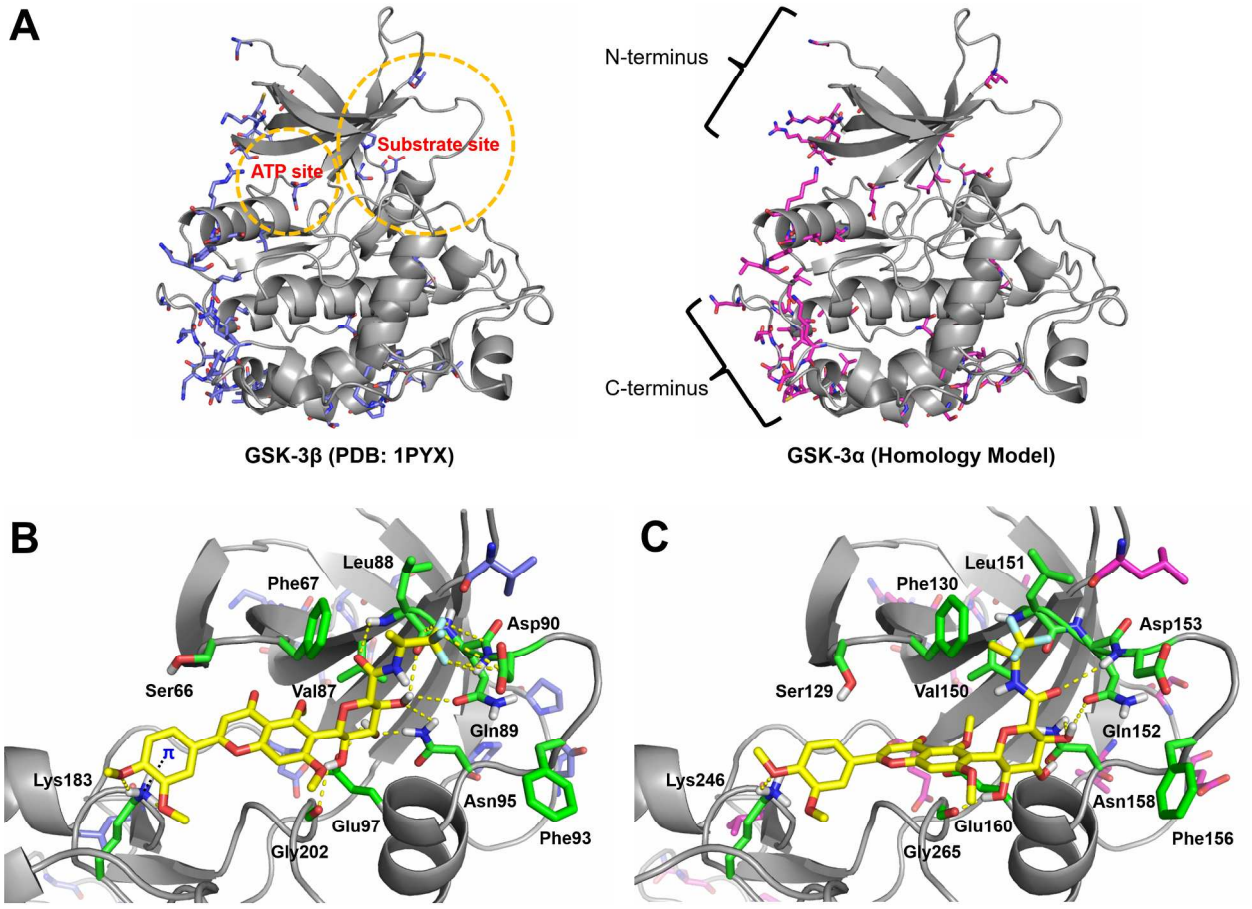

Figure 7. Molecular models of GSK-3β and GSK-3α and the docking complexes with **30**. (A) Superposition of GSK-3β structure (PDB code 1PYX) and GSK-3α homology model (UniProt code P49840). The ATP and substrate sites are highlighted in circles, and the N- and C-termini are depicted. The ATP and substrate sites of GSK-3α/β isoforms are highly conserved and most of amino acid differences occur in the N- and C-terminal regions. (B) Predicted docking pose of **30** into the substrate site of GSK-3β structure. (C) Predicted docking pose of **30** into the substrate site of GSK-3α homology model. GSK-3 isoforms are shown as gray cartoons. In both isoforms, selected conserved residues are displayed as green sticks. In GSK-3β, non-conserved residues are displayed as blue sticks. In GSK-3α, non-conserved residues are displayed as magenta sticks. The dotted lines represent key molecular interactions.

1144 For Table of Contents Use Only

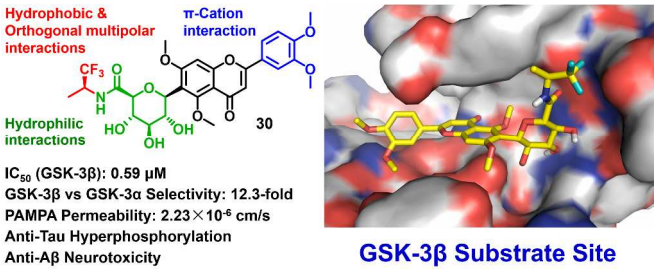

Title: Discovery of Selective, Substrate-Competitive, and Passive Membrane Permeable Glycogen Synthase Kinase-3β Inhibitors: Synthesis, Biological Evaluation, and Molecular Modeling of New *C*-Glycosylflavones

Authors: Zhibin Liang and Qing X. Li